공학석사 학위논문

Structural Safety Assessment of Offshore Equipment Safety Barrier with Weight Impact

중량물 충돌에 의한 해양플랜트 장비 보호용 방호벽의
구조 안전성 평가

지도교수 이 상 갑

2017 년 2 월

한국해양대학교 대학원

조선해양시스템공학과
조 재 상

본 논문을 조재상의 공학석사 학위논문으로 인준함.

위원장	박 석 주	(인)
위 원	이 상 갑	(인)
위 원	남 종 호	(인)

2017 년 2 월

한국해양대학교 대학원

Table of Contents

List of Tables

List of Figures

중량물 충돌에 대한 해양플랜트 장비 보호용 방호벽의 구조 안전성 평가

조 재상

한국해양대학교 대학원
조선해양시스템공학과

초록

최근 선박 및 해양플랜트 상에서 크레인을 이용한 선적화물 탑재 중 중량물이 선체 및 주요 장비에 충돌하는 사고가 빈번하게 발생하고 있으며, 사고 방지를 위하여 방호벽(Safety Barrier)이 주요장비를 둘러싸도록 설치된다. 이 구조물은 충돌 발생 시 최고 경사각도 14도 이상 넘어가지 않아야 하며 충돌 후에 원위치로 복귀되어야 한다. 본 연구에서는 방호벽에 중량물이 충돌하였을 경우의 거동 특성을 파악하기 위하여 LS-DYNA 코드를 이용하여 중량물 충돌에 대한 내충격 응답해석 기법을 개발하여 중량물 충돌의 충격 시험 결과와 검증하였다. 유압댐퍼(hydraulic damper)의 감쇠점성(damping viscous)과 충돌 접촉(contact) 시의 감쇠계수(damping coefficient) 등을 실제 충돌 시의 거동과 잘 맞도록 추정하였다. 예측되는 충돌상황의 시나리오를 설정하여 장비 보호용 방호벽의 성능을 검토하고 구조 안정성 평가를 수행하였으며 충분한 강도를 확보하였음을 확인할 수 있었다.

1. Introduction

The size of ship and offshore structures has been increased according to the worldwide increasing demands of the quantity of good transportation and large storage capacity of oil and gas, such as jack-up, drill ship, semi-rig, FPSO, etc., as shown in Fig. 1.1. Many cargos, such as containers and drill pipes, etc., have been lifted and moved on the upper deck of ship and topside of offshore structure, as their demands. Unexpected cargo crash accidents frequently occurred with main equipments on their upper deck and topside, during cargo lifting operations. Since these impact accidents generally lead to serious damage to the main equipments and hull structure, safety barrier should be installed around the main equipments for their protections, as shown in Fig. 1.2.

Fig. 1.1 Typical offshore structures

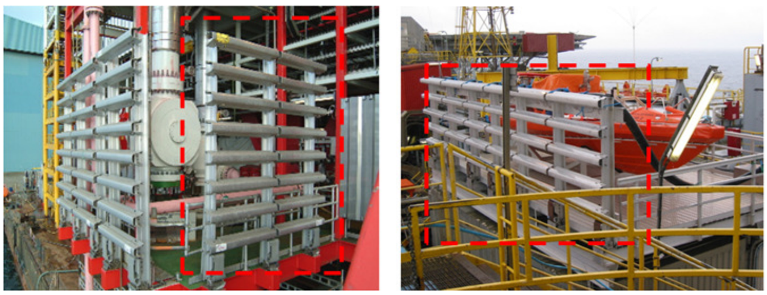

Fig 1.2 Installation of safety barrier on upper-deck and topside

This safety barrier usually has 2~8 layered guide rails according to the height of equipments, and should absorb the sudden impact shocks, with the satisfaction of its structural safety requirement against the crash impacts. As shown in Figs. 1.3 and 1.4, the safety barrier should be back to the its original position by its hydraulic spring-damper system, and be inclined to the small angle under 14° (KOMERI, 2016) during cargo impact to equipments. For its safety requirement, reasonable and reliable structural safety should be guaranteed, and impact force criteria should be also set up based on its safety requirement.

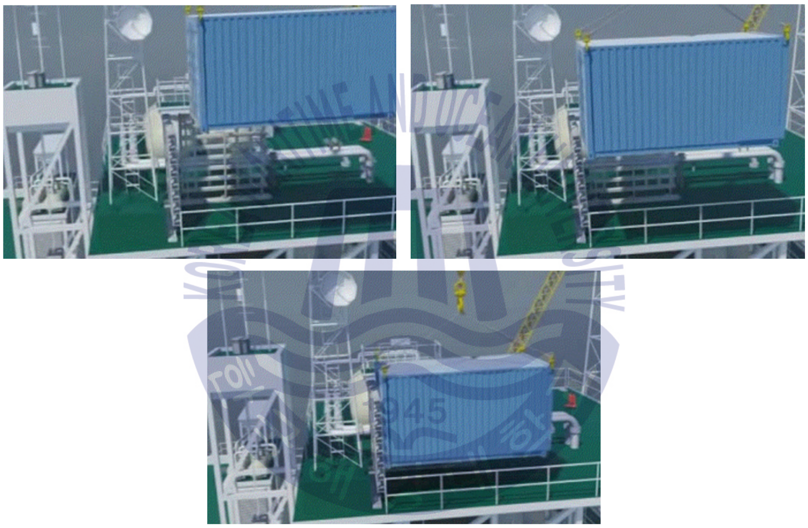

Fig 1.3 Operation photo of safety barrier on offshore topside

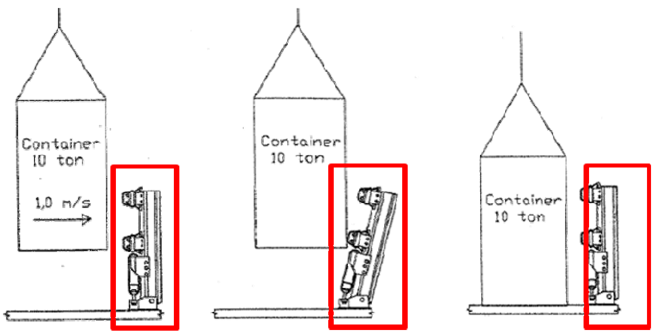

Fig. 1.4 Operation condition of safety barrier on offshore topside

The original 8 layered safety barrier, as shown in Fig. 1.5(a), has been developed and modified with two points, as shown in Fig. 1.5(b), such as material change from steel to aluminum for weight reduction, and rubber type damper to hydraulic spring-damper type absorber for the maintenance reduction due to the short life period of rubber hardening characteristics in ocean environment. Whereas the skill of strength design should be secured for the strength reduction due to the light material application, the hydraulic spring-damper absorber, as shown in Fig. 1.6, could make up for the strength reduction weak point of light material.

(a) original safety barrier (b) developing safety barrier

Fig 1.5 Original and developing 8 layered safety barriers

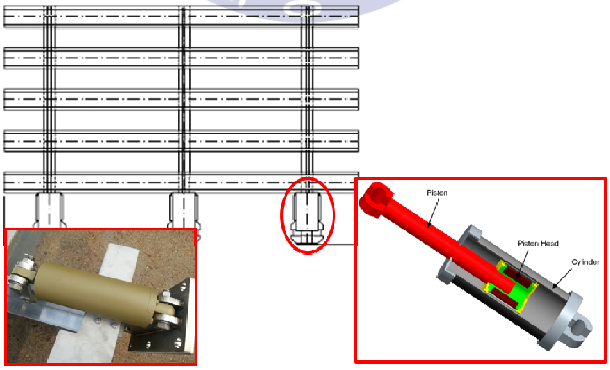

Fig 1.6 Developing safety barrier with hydraulic spring-damper absorber

For the reasonable and reliable structural safety assessment of developing safety barrier, the impact response analysis technique using LS-DYNA code (LSTC, 2013) was verified through the impact test result. For the safety barrier impact test, the impact medium was suspended with ropes to the crane and was swung to the safety barrier with 5.0kJ impact energy. The most frequent crash accident case was implemented to the impact test. In the real impact test, the impact medium was rotated a little bit during initial stage, and a lot during the second stage. Impact response analyses were carried out with and without the consideration of impact medium rotation, for the accurate comprehension of impact response of safety barrier.

The objective of this study is to develop a more accurate and realistic impact response analysis technique of safety barrier with hydraulic spring-damper absorbers for the structure safety assessment of safety barrier and its improvement to the impact accidents, using LS-DYNA code, by the verification of impact test result and the consideration of diverse impact response analysis scenarios.

2. Impact Test of Safety Barrier

In the impact test of safety barrier, impact medium with its weight 5.245ton was suspended with steel ropes to the crane with height 20.0m including its medium height, and was pulled back behind 1.97m with height 0.097m for the securing of impact energy 5.0kJ by forklift and was suspended with steel ropes to the crane and was swung to the safety barrier with 5.0kJ impact energy, as shown in Fig. 2.1 (KOMERI, 2016).

Fig 2.1 Impact test scenario of safety barrier (KOMERI, 2016)

The impact energy 5.0kJ has been selected by the most frequent lifting case of the container, with its size 3,048mm × 2,438mm × 2,621mm, its maximum gross weight 10.115ton, and its normal transportation speed 1.0m/sec, on the upper deck and topside. Since it was difficult to implement the realistic impact test condition, the same manner was applied to the impact response analysis with the same potential energy 5.0kJ, as shown in Table 2.1. Inclined angle should be measured for the performance verification of safety barrier, during the impact test, and the angle measured sensors were mounted at the bottom of 4 columns of safety barrier, as shown in Fig. 2.2.

Table 2.1 Impact test specifications of developing safety barrier

parameter		specification
target container	weight (ton)	10.115
	travelling speed (m/s)	1.000
impact medium	weight (ton)	5.245
	impact energy (kJ)	5.000
	lifting height (m)	0.097
	pulling back distance (m)	1.970

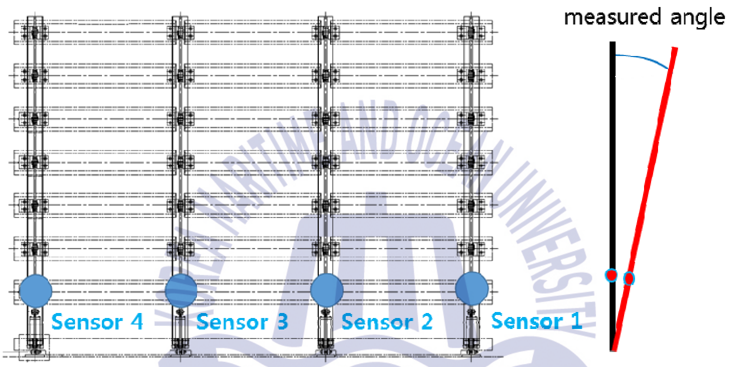

Fig 2.2 Angle measured sensor positions at safety barrier in impact test

The maximum inclined angle and final restored one of the safety barrier were measured and recorded during and after impact test of developing 8 layered safety barrier. Authorized expert checked whether the cracks were generated or not on the foundations. The following five points were checked for reasonable and reliable impact test: First of all, the aluminum safety barrier and impact medium were aligned at the reference location (zero point). Secondly, the impact medium was pulled back behind to generate the impact energy of 5.0kJ by forklift towing. Thirdly, the height 0.097m of impact medium was measured from the reference location at the maximum backward pullback distance 1.970m. Fourthly, forklift was moved backward very fast to the sufficient distance for the prevention of impact medium from the forklift and safety barrier. Finally, authorized expert checked the crack generations on the foundations.

The logicality of the impact test measurements was also examined throughly based on the following three check points: First of all, impact test measurements were kept until the vibration of the impact medium would stop. Secondly, inclined angles were measured with developing measuring equipment at every 0.1 second for each sensor in real time. Thirdly, the maximum and minimum inclined angles were shown by the program, where the maximum and minimum angles indicated the maximum inclined angle at the impact test, and the restored one after stopping the vibration of the impact medium. Figure 2.3 shows the overall impact test process and operation of the safety barrier.

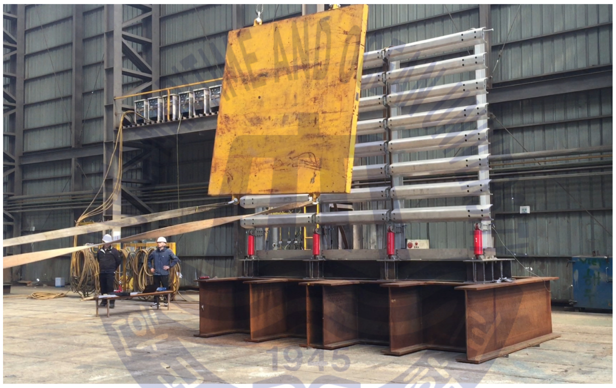

Fig 2.3 Overall view of impact test process and operation of safety barrier

As the impact test result, the inclined angles were only measured at every 0.1 second with four sensors, and the plastic deformation and fracture could be checked by the visual identification and there was no plastic damage. The impact test results were used for the reference of the impact response analysis of safety barrier. Figure 2.4 shows the inclined angle responses of the impact test of aluminum safety barrier. From the inclined angle response, it could be found that the maximum inclined angles were generally smaller than the limitation angle 14° (DNVGL, 2010; KOMERI, 2016), and that the hydraulic spring-damper absorbers performed their roles to prevent the over return back of the safety barrier to original position. There was no the physical plastic damage in the safety barriers and absorbers. From the examination of performance of the safety barrier from the impact test, the safety barrier could have enough structural strength in this impact test.

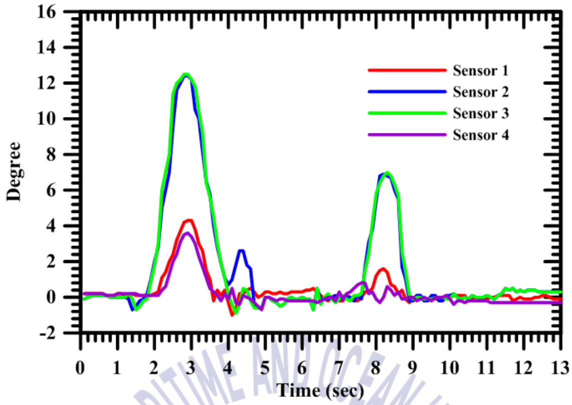

Fig 2.4 Inclined angle responses of safety barrier in impact test

The impact test process could be divided largely into four steps, as shown in Fig. 2.5. From 0.00sec to 2.14sec, it was waiting time on the top position for securing potential energy and right before impacting time of the impact medium to the safety barrier. The first impact time was from 2.14sec to 3.96sec, and then rebounding time was from 3.96sec to 7.75sec. The second impact occurred during 7.75sec~8.82sec. Steady condition occurred after the impacts. The impact test process scenes are shown in Fig. 2.5 with time interval.

(a) swing to 1st impact (0.00s~2.14s)

(b) 1st impact (2.14s~3.96s)

(c) rebounding after 1st impact (3.96s~7.75s)

(d) 2nd impact (7.75s~8.82s)

(e) 3rd impact & steady (8.82s~13.00s)

Fig 2.5 Impact test process scenes of safety barrier and impact medium

3. Impact Simulation Modeling and Scenarios

The impact simulation was performed for the verification of the impact test result of the aluminum safety barrier, and its modeling and scenarios are considered.

3.1. Impact simulation modeling

The overall Finite Element configuration of impact simulation model of the safety barrier with impact medium in the impact test is shown in Fig. 3.1. The impact simulations were carried out with the consideration of gravity of safety barrier and impact medium. Figure 3.2 illustrates the Finite Element configuration of impact medium model with its dimension ($2.50m \times 2.45m \times 0.109m$ in length, height and thickness), its volume ($0.668m^3$) and weight (5.245ton). Its shell mesh size was 40.0mm, and was suspended by steel ropes to the top side of crane with the heigh 20.0m including the height of impact medium. The lower of impact medium was pulled back behind 1.970m in the x-direction.

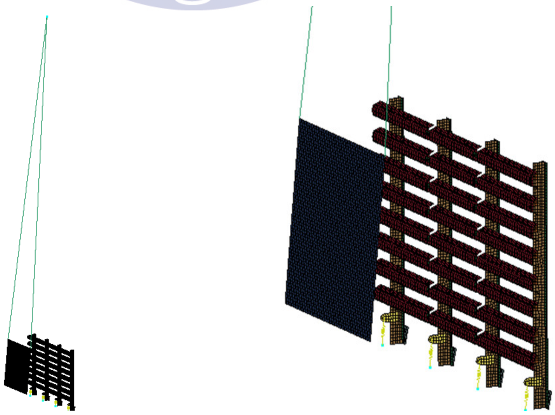

Fig 3.1 Overall and close views of Finite Element configurations of safety barrier impact simulation

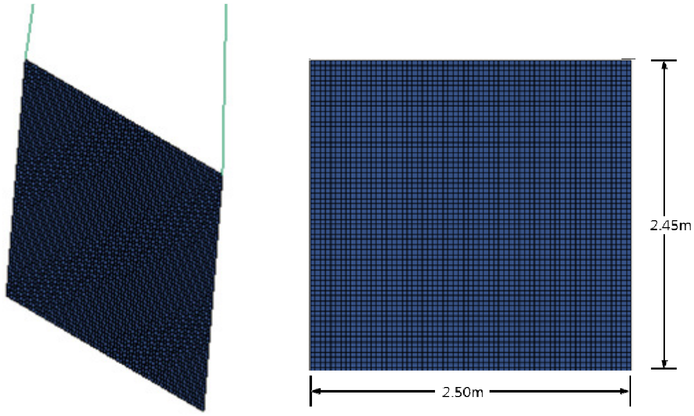

Fig 3.2 Finite Element configuration and dimension of impact medium

Figure 3.3 shows the Finite Element configuration and dimension of safety barrier, where its dimension was $4.25\text{m} \times 3.30\text{m} \times 0.210\text{m}$ in length, height and width, its mesh size was 40mm, and the bottom of safety barrier columns are inclined rotation free along the length of safety barrier, y-axis direction. Figures 3.4~3.6 describe the detailed Finite Element configurations of guide rails, columns and hydraulic spring-damper absorber, and their mesh sizes were 40mm, which are the principle components of the safety barrier. An elasto-plastic material, MAT_PLASTIC_KINEMATIC (MAT_03), was used for the guide rails and columns in the impact simulation, and MAT_SPRING_ELASTIC (MAT_S01) and MAT_DAMPER_VISCOUS (MAT_S02) were used for the spring and damper components of hydraulic absorber, respectively. Figure 3.7 illustrates the spring nonlinear constant curve from 2,941N at 0.0mm to 10,541N to 55.0mm provided by the production company (SEBOTECH, 2016). Shell elements were used for the safety barrier and impact medium with around the numbers 21,810 and 3,844, respectively.

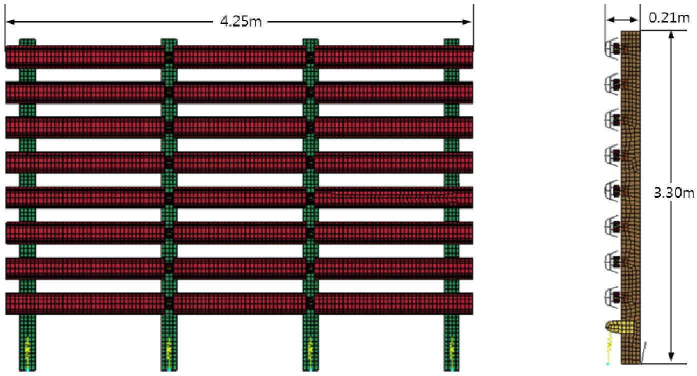

Fig 3.3 Finite Element configuration and dimension of safety barrier

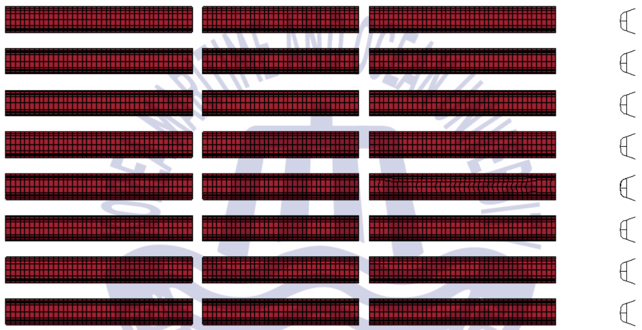

Fig 3.4 Finite Element configuration of guide rails in safety barrier

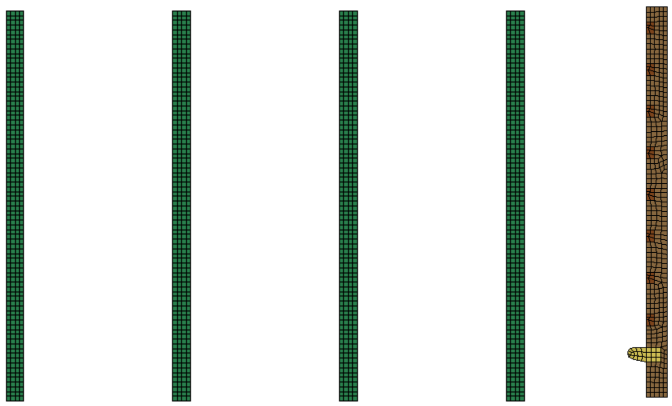

Fig 3.5 Finite Element configuration of columns in safety barrier

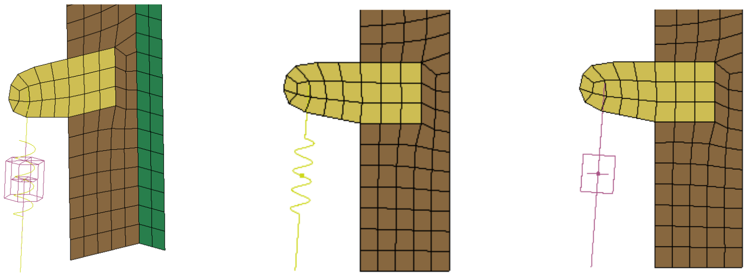

Fig 3.6 Finite Element configuration of hydraulic spring-damper absorber

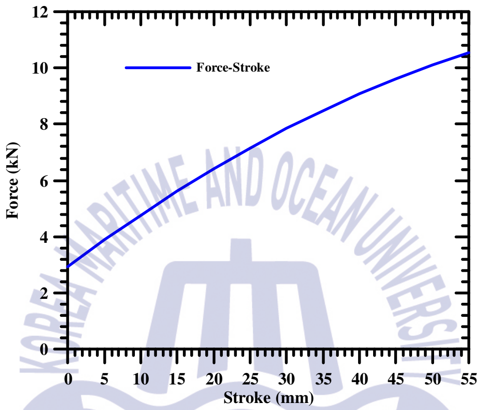

Fig 3.7 Force-Stroke curve of spring in hydraulic spring-damper absorber (SEBOTECH, 2016)

The material properties, such as SUS316 and 6082-T6 aluminum alloy (British Standard, 2007), are shown in Table 3.1, where the material of guard rails and columns of safety barrier was 6028-T6 aluminum alloy, and impact medium one, SUS316. As mentioned before, the impact simulations were carried out for the structural safety assessment of the safety barrier in the crash accidents. For the future study, structural safety assessment will be performed for the diverse safety barriers, and impacting bodies, such as containers and main equipments, etc. Structural safety assessment of the safety barrier was carried out based on the strength evaluation of each component of safety barrier, where their maximum stresses of guard rails and columns were compared with reference Von-mises effective stress, and their maximum deformations of hydraulic spring-damper absorber, with reference displacement.

Table 3.1 Material properties of safety barrier

property	SUS316	6082-T6
Young's modulus (GPa)	200	70
Poisson's Ratio	0.3	0.33
Density (kg/m^3)	7,850	2,700
Yield stress (MPa)	205	260
Ultimate stress (MPa)	520	310

3.2. Impact simulation scenarios

It was figured out that the impact medium was rotated a little bit during hitting to the safety barrier because of the very small difference of wire release time in the impact test. In Case 1, as shown in Fig. 3.8, diverse rotation angles, 0.5°~2.0°, were tried for the verification of impact simulation using LS-DYNA code with comparison of impact test results. In addition to the spring nonlinear constant curve of the hydraulic absorber, Fig. 3.7, diverse damping constants, such as damping viscous of damper in hydraulic absorber and damping coefficient in contact option between the safety barrier and impact medium, were also tried for its verification. This verification of impact simulation could guarantee the reasonable and accurate structural safety assessment for the diverse impact loading conditions, such as the height and side impact positions of impact medium to the safety barriers. Unforeseeable circumstances in safety barrier would be expected according to the impact loading positions of the impact medium. The impact behavior of the safety barrier could be very different depending on impact position due to the unforeseeable circumstances motion on the upper deck and topside, so diverse simulations have been carried out according to the impact position. Cases 2~5, as shown in Figs. 3.9~3.12, were treated as the impact simulation scenarios.

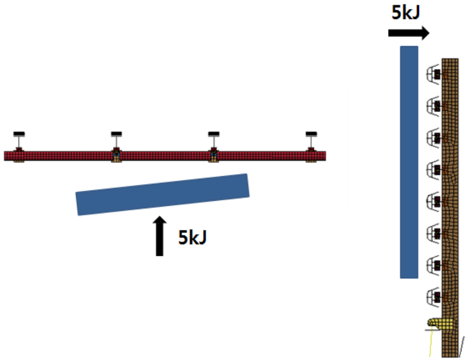

Fig 3.8 Impact simulation scenario Case 1 of safety barrier in test condition

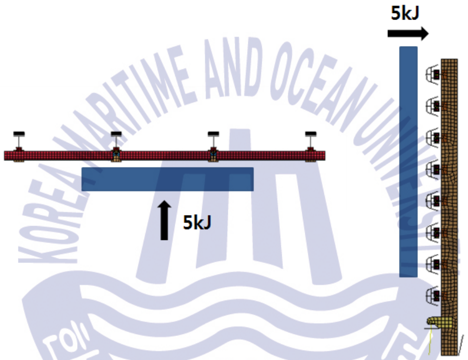

Fig 3.9 Impact simulation scenario Case 2 of safety barrier with impact medium at center, normal height and no rotation

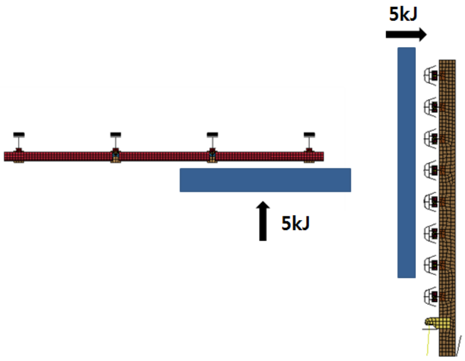

Fig 3.10 Impact simulation scenario Case 3 of safety barrier with impact medium at side, normal height and no rotation

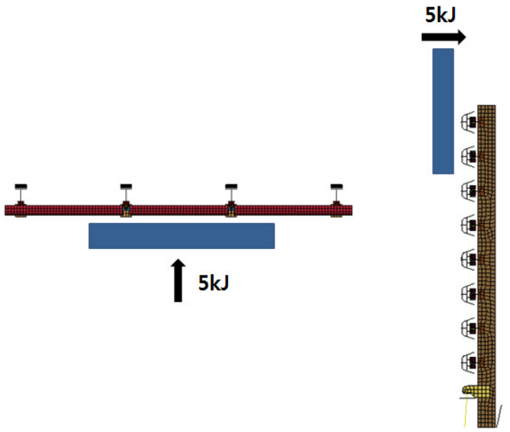

Fig 3.11 Impact simulation scenario Case 4 of safety barrier with impact medium at center, upper height and no rotation

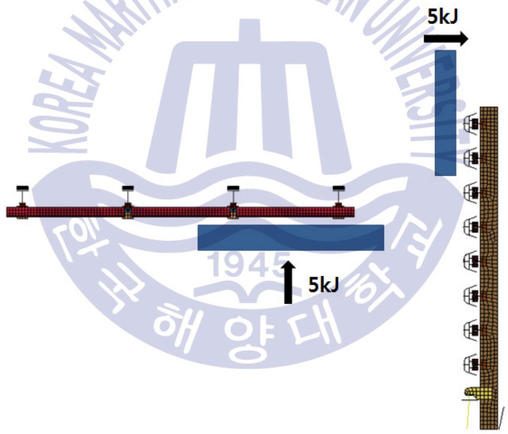

Fig 3.12 Impact simulation scenario Case 5 of safety barrier with impact medium at side, upper height and no rotation

4. Impact Simulation of Safety Barrier

Diverse impact simulations of the safety barrier were carried out according to scenario, such as Cases 1~5 in Figs. 3.8~3.12. As mentioned in section 3.1, verification of the impact simulation of the safety barrier was performed in Case 1 by the comparison of the impact simulation results with impact test one, such as the inclined angle response.

4.1. Impact simulation of scenario Case 1 (impact test condition)

At first, impact simulation of Case 1 was carried out just using spring component in hydraulic spring-damper absorber, with spring nonlinear constant curve, as shown in Fig. 3.7. The inclined angle response of absorber Sensor 3 is shown in Fig. 4.1, and the front, top and side views of the impact simulation behaviors are shown in Figs. 4.2~4.4, respectively. As expected, severe oscillation impact behaviors in the safety barrier and inclined angle response of Sensor 3 occurred, 4 times with around 1.0sec interval from 4.02sec to 7.92sec right after the first impact peak and duration. As the 2nd impact of the impact medium occurred to the safety barrier after 8.03sec, oscillation became reduced and safety barrier was returned to the steady position around after 9.6sec. Whereas its first inclined angle response was almost the same as the test one in the first impact peak and duration, no coincidence of inclined angle response occurred after the 1st impact. It could be found that damping component of hydraulic absorber and damping effect between the safety barrier and impact medium would be considered for the stable behavior and response.

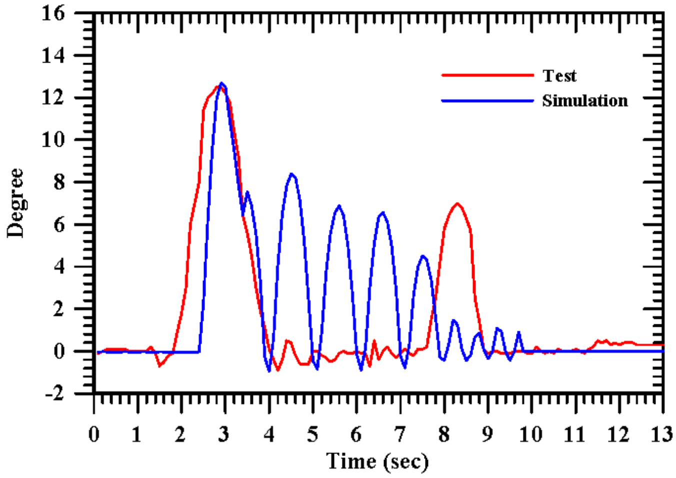

Fig 4.1 Comparison of inclined angle response of Sensor 3 between impact simulation and test with only hydraulic spring absorber

(a) swing to 1st impact (0.00s~2.43s)

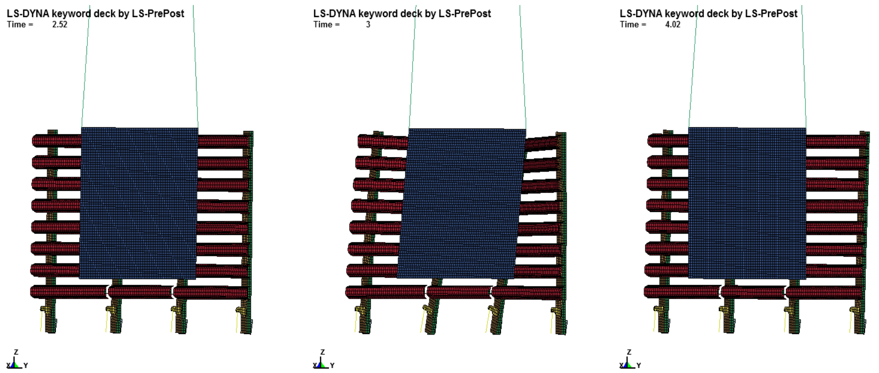

(b) 1st impact (2.43s~4.02s)

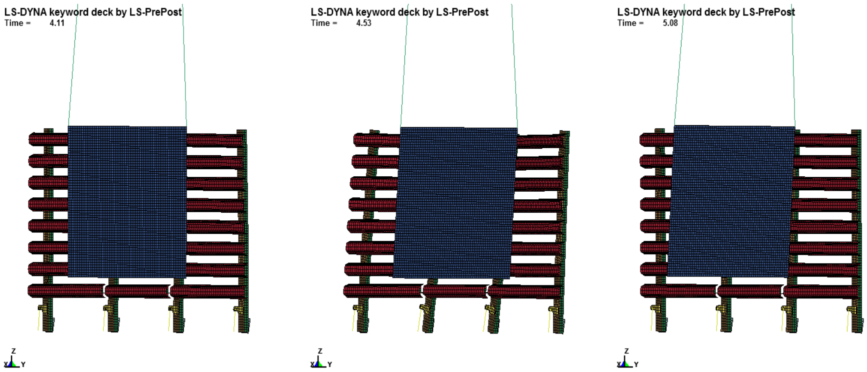

(c) 1st oscillation (4.02s~5.08s)

(d) 2nd oscillation (5.08s~6.03s)

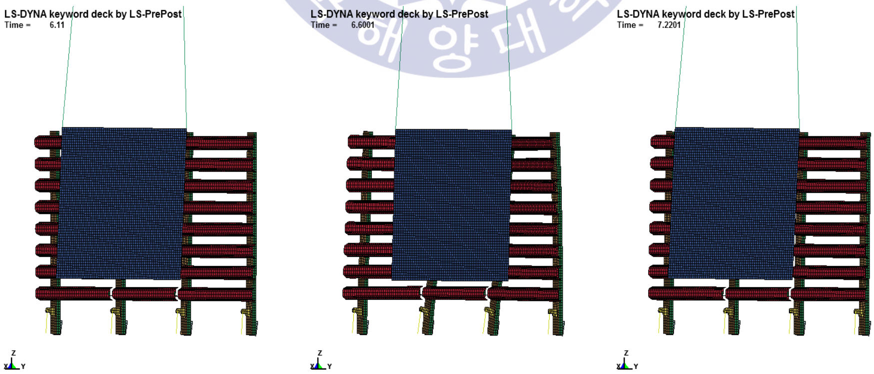

(e) 3rd oscillation (6.03s~7.22s)

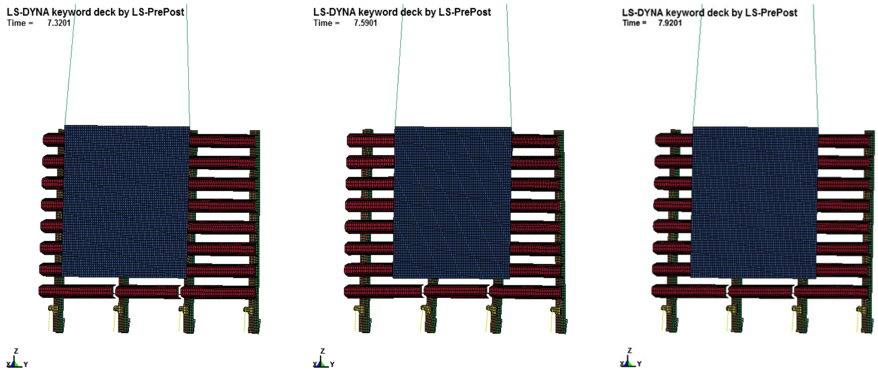

(f) 4th oscillation (7.22s~7.92s)

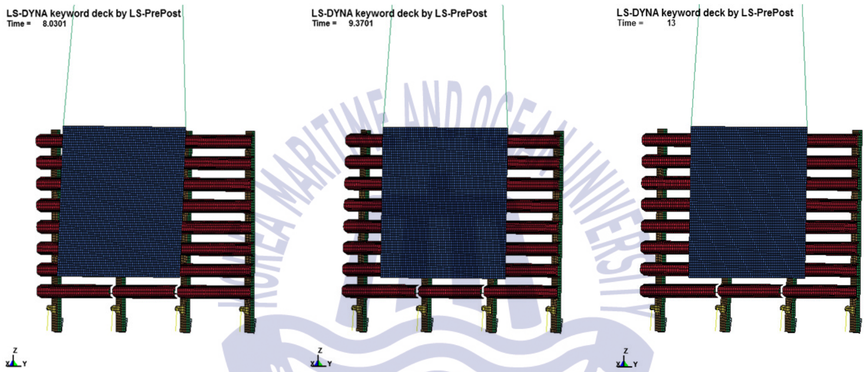

(g) 2nd impact & steady (7.92s~13.00s)

Fig 4.2 Front view of impact simulation behavior of safety barrier and impact medium with only hydraulic spring absorber

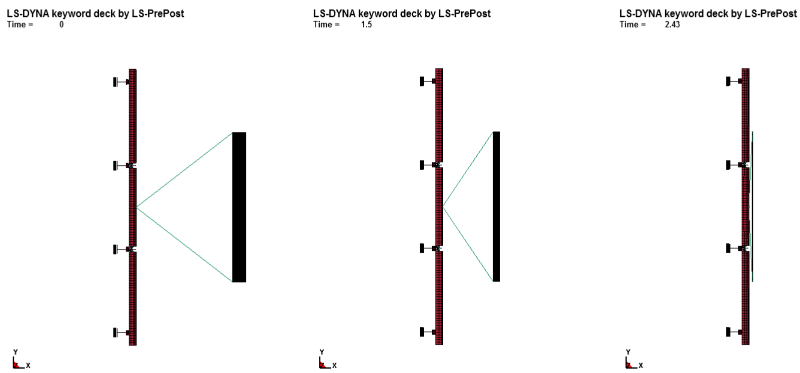

(a) swing to 1st impact (0.00s~2.43s)

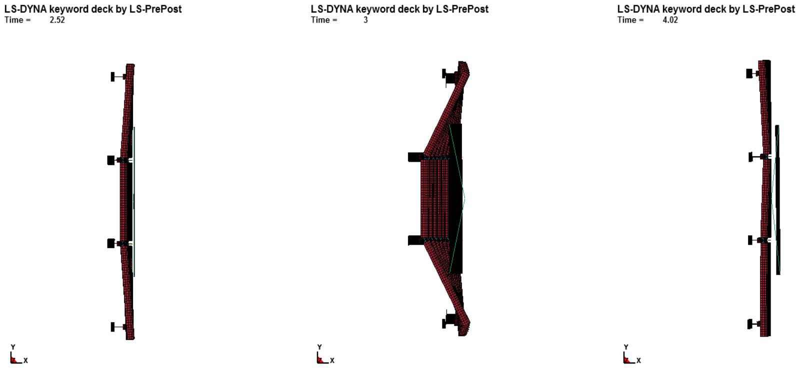

(b) 1st impact (2.43s~4.02s)

(c) 1st oscillation (4.02s~5.08s)

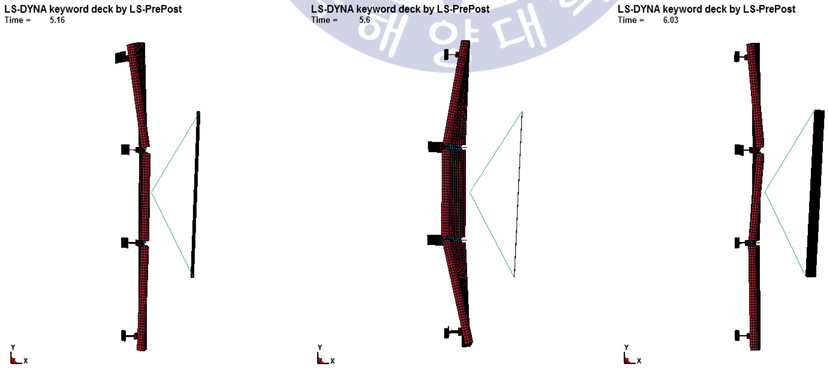

(d) 2nd oscillation (5.08s~6.03s)

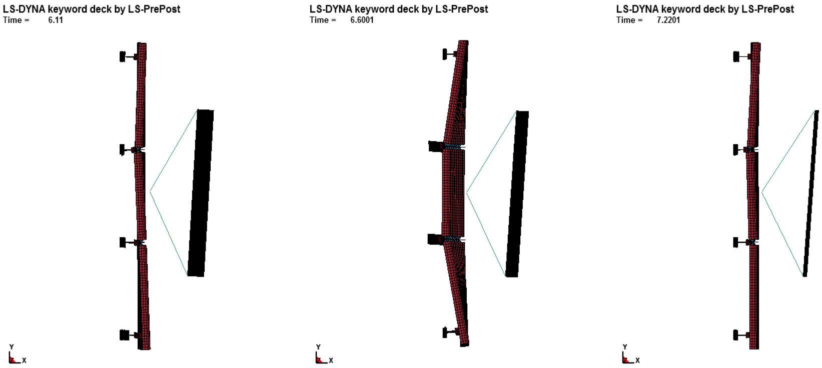

(e) 3rd oscillation (6.03s~7.22s)

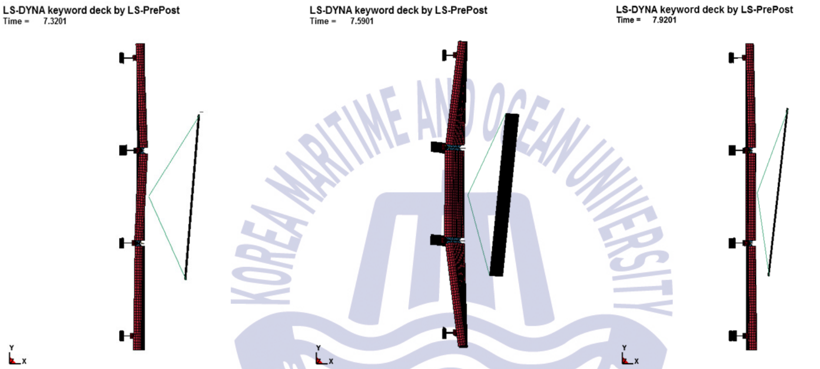

(f) 4th oscillation (7.22s~7.92s)

(g) 2nd impact & steady (7.92s~13.00s)

Fig 4.3 Top view of impact simulation behavior of safety barrier and impact medium with only hydraulic spring absorber

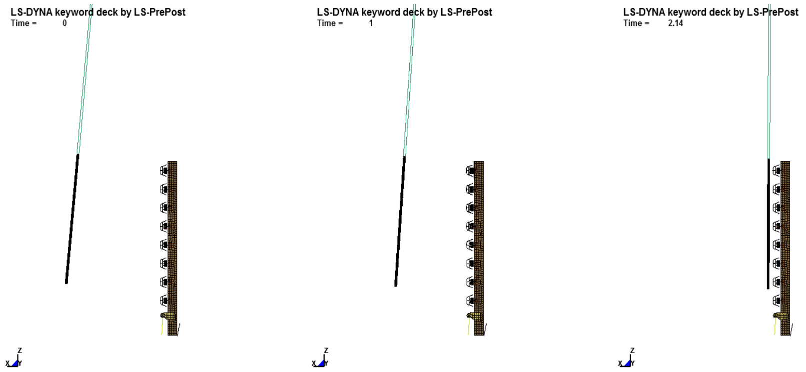

(a) swing to 1st impact (0.00s~2.14s)

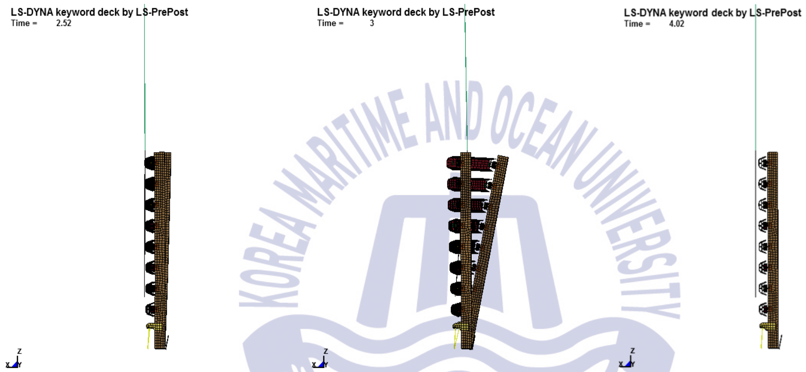

(b) 1st impact (2.14s~4.02s)

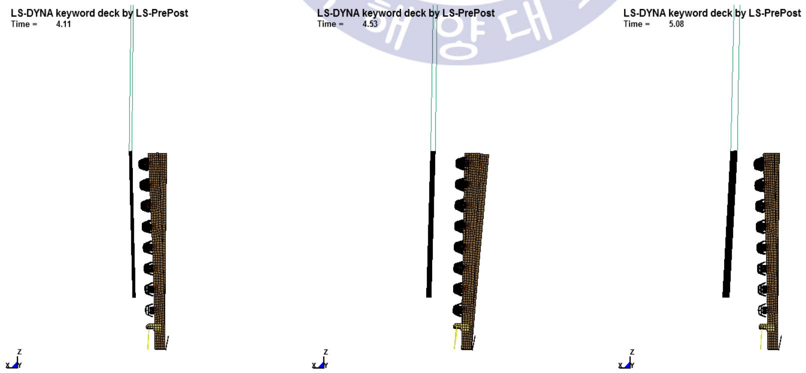

(c) 1st oscillation (4.02s~5.08s)

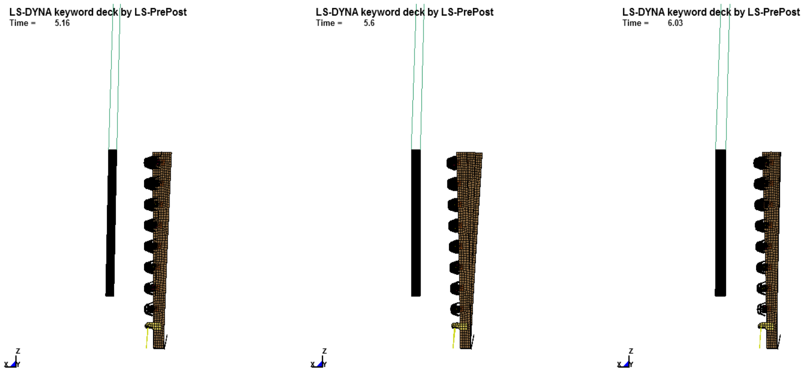

(d) 2nd oscillation (5.08s~6.03s)

(e) 3rd oscillation (6.03s~7.22s)

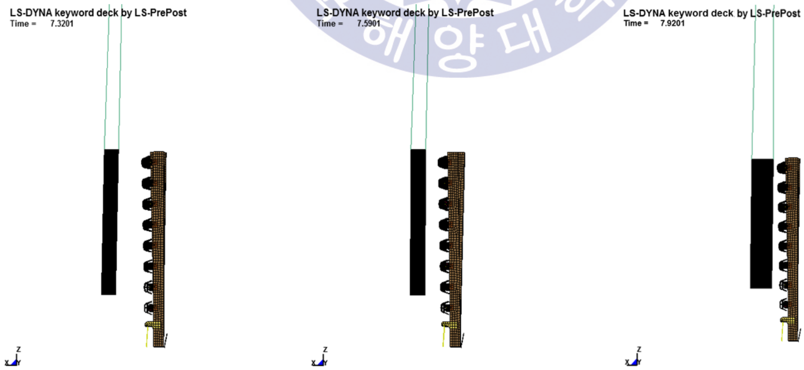

(f) 4th oscillation (7.22s~7.92s)

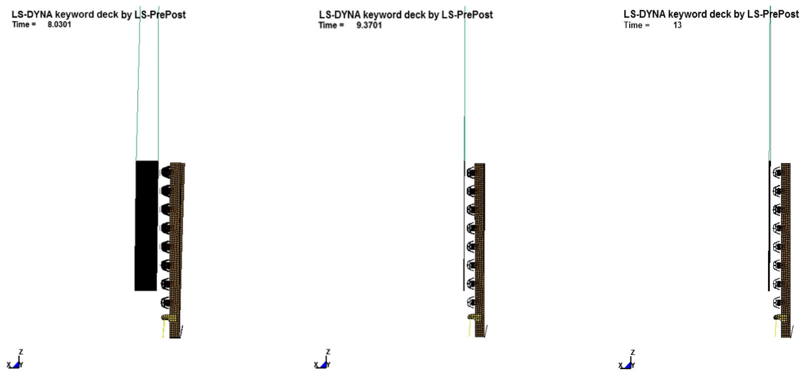

(g) 2nd impact & steady (7.92s~13.00s)

Fig 4.4 Side view of impact simulation behavior of safety barrier and impact medium with only hydraulic spring absorber

This severe oscillation behavior and response after the first impact period could be due to the no consideration of damper component in the hydraulic spring-damper absorber and damping effect between the safety barrier and impact medium in the impact simulation. Impact simulations were carried out for the verification of the impact test considering diverse damping viscous values of damper, 1.0×10^5N/mm·s, 7.5×10^4N/mm·s and 5.0×10^4N/mm·s for MAT_DAMPER_ VISCOUS option and diverse damping coefficients, 0.1, 0.05 and 0.03, for the AUTO_SURFACE_TO_SURFACE contact option between the safety barrier and impact medium. Figure 4.5 shows the inclined angle responses of Sensors 1~4 in impact simulations compared to the impact test one according to damping viscous value with damping coefficient 0.1. It could be found that the inclined angle responses of Sensors 1~4 in impact simulations were roughly close to the impact test ones in the 1st impact period, and that their damping responses to the 2nd period, also generally close to the impact test one. However, these response seems to be far from the more close responses to the impact test ones, and diverse damping coefficients were considered to the previous damping viscous values.

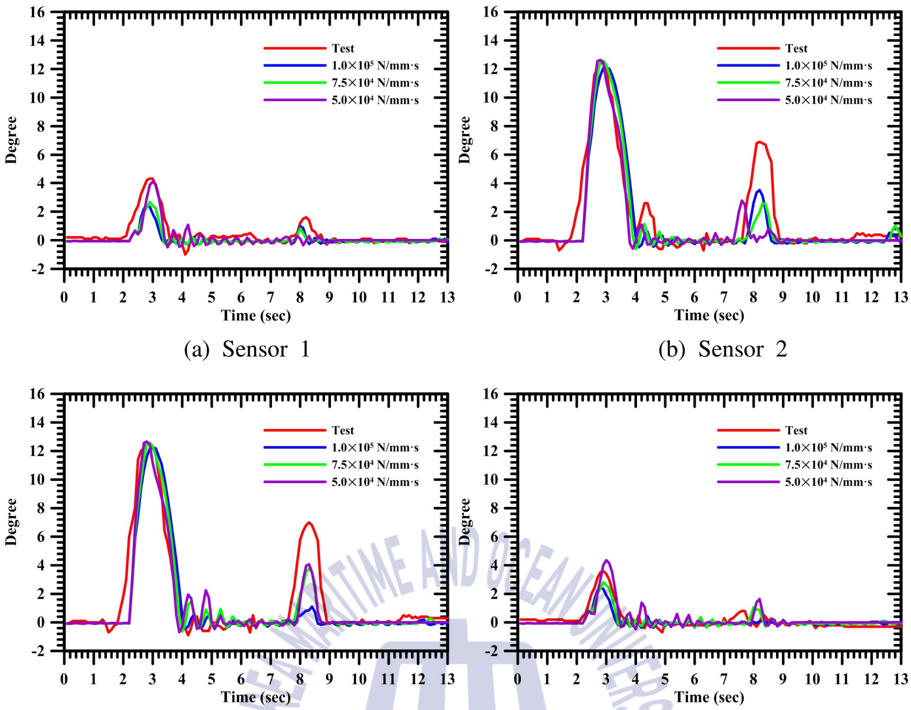

(a) Sensor 1 (b) Sensor 2

(c) Sensor 3 (d) Sensor 4

Fig 4.5 Comparison of inclined angle responses of Sensors 1~4 between impact simulations and test according to damping viscous with damping coefficient 0.1

Figure 4.6 also illustrates the inclined angle responses of Sensors 1~4 in impact simulations compared to the impact test one according to damping coefficient value, 0.1, 0.05 and 0.03, with damping viscous value 7.5×10^4N/mm·s. It could be found that the inclined angle responses of Sensor 1~4 in impact simulations would be generally more close to the impact test one with damping coefficient 0.03, where their inclined angle responses in only Case 1 are replotted in Fig. 4.7 and their maximum inclined angles at the 1st and 2nd impact peaks are summarized with test ones in Table 4.1. Their maximum inclined angles were smaller than the limitation angle 14°. Figures 4.8~4.10 show the front, top and side views of the impact simulation behaviors of the safety barrier and impact medium of scenario Case 1, and it could be found that their simulation behaviors are in good agreement with the test ones.

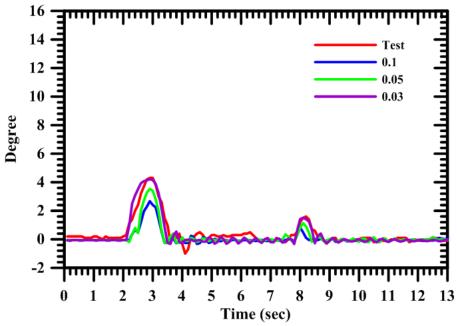

(a) Sensor 1

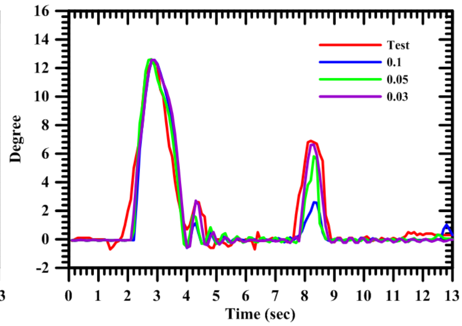

(b) Sensor 2

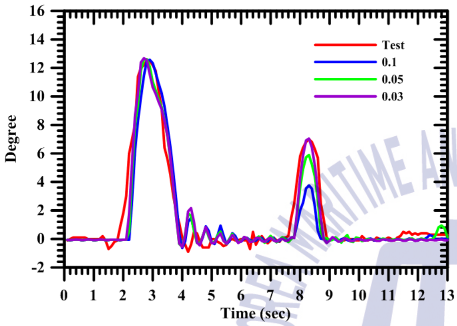

(c) Sensor 3

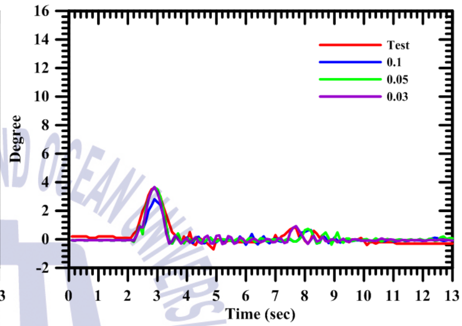

(d) Sensor 4

Fig 4.6 Comparison of inclined angle responses of Sensor 1~4 between impact simulations and test according to damping coefficient value with damping viscous 7.5×10^4N/mm·s

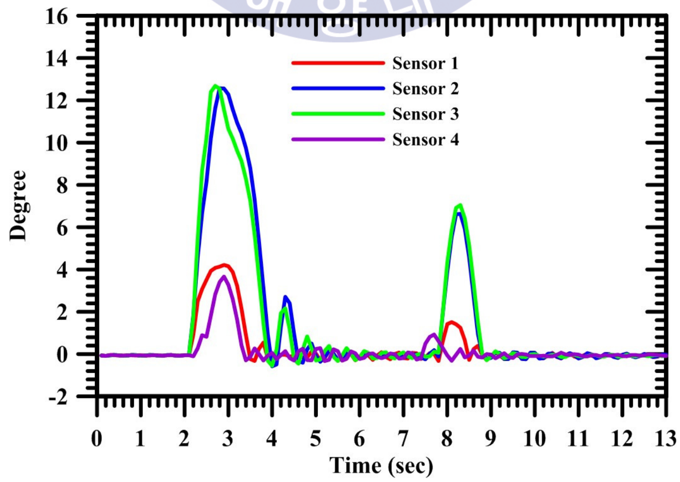

Fig 4.7 Inclined angle responses of Sensors 1~4 in scenario Case 1

Table 4.1 Maximum inclined angles of Sensor 1~4 with damping viscous 7.5×10^4N/mm·s and damping coefficient 0.03 (Case 1) and test ones

Sensor	Impact peak	Case 1 (°)	test (°)
1	1st	4.21	4.30
	2nd	1.51	1.60
2	1st	12.57	12.60
	2nd	6.83	6.90
3	1st	12.68	12.70
	2nd	7.05	7.00
4	1st	3.67	3.60
	2nd	0.93	0.90

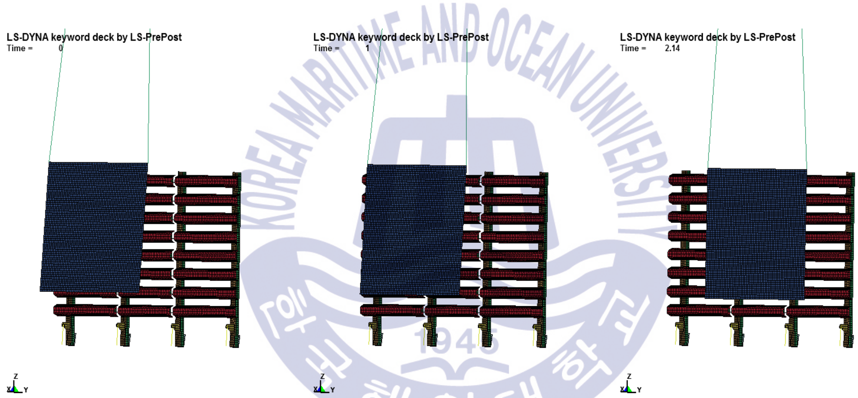

(a) swing to 1st impact (0.00s~2.14s)

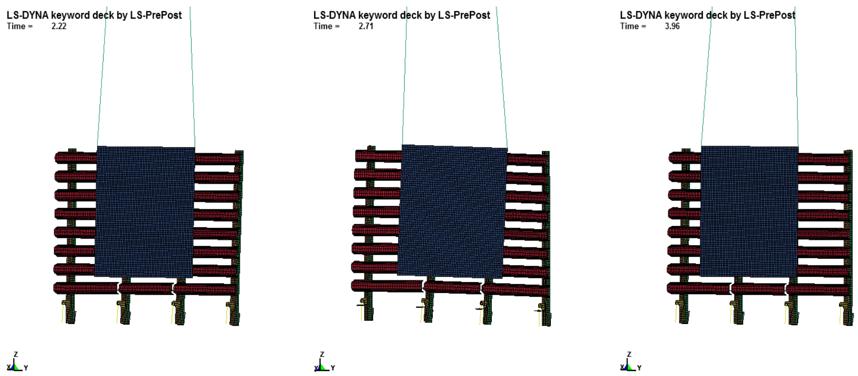

(b) 1st impact (2.14s~3.88s)

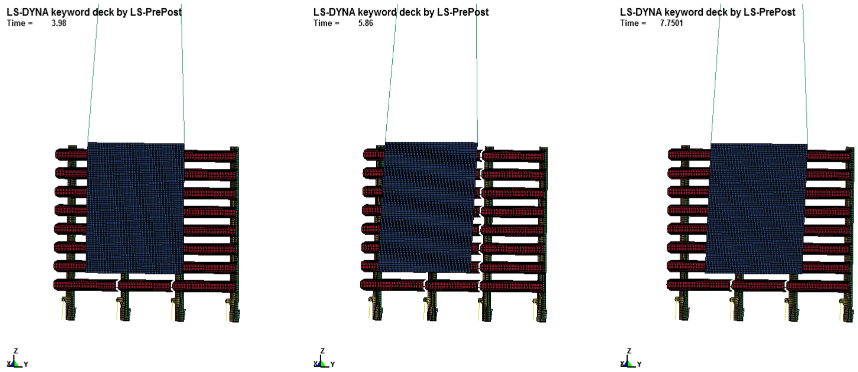

(c) rebounding after 1st impact (3.88s~7.64s)

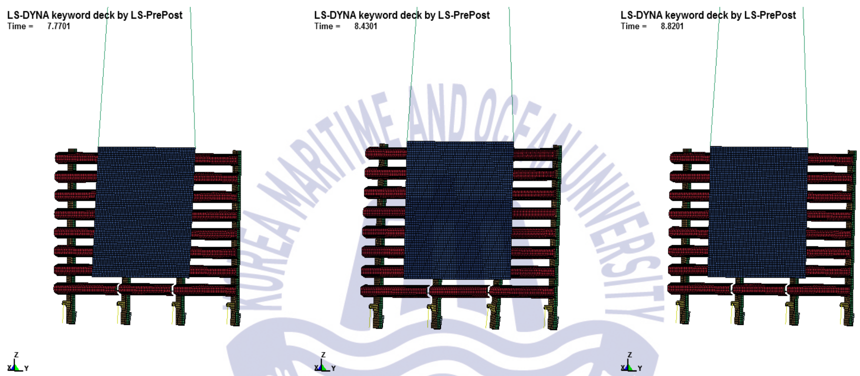

(d) 2nd impact (7.64s~8.82s)

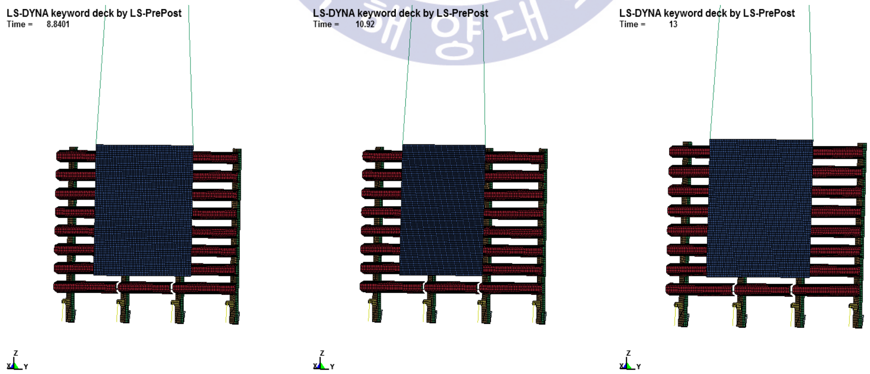

(e) 3rd impact & steady (8.82s~13.00s)

Fig 4.8 Front view of impact simulation behavior of safety barrier and impact medium in Case 1

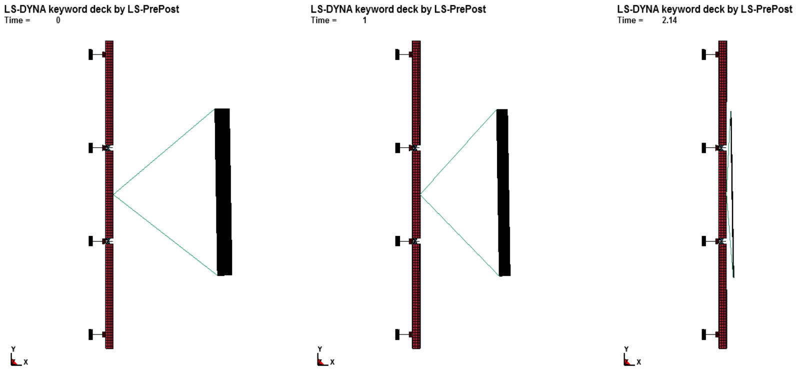

(a) swing to 1st impact (0.00s~2.14s)

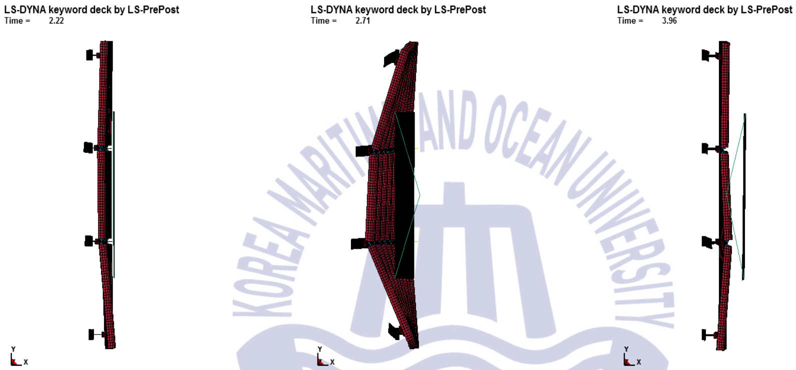

(b) 1st impact (2.14s~3.96s)

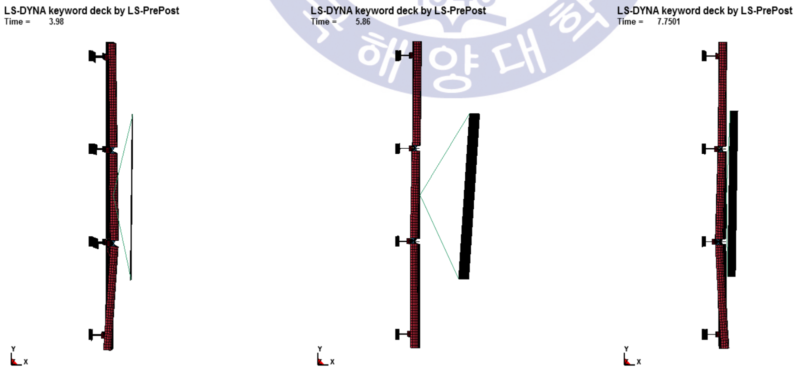

(c) rebounding after 1st impact (3.96s~7.75s)

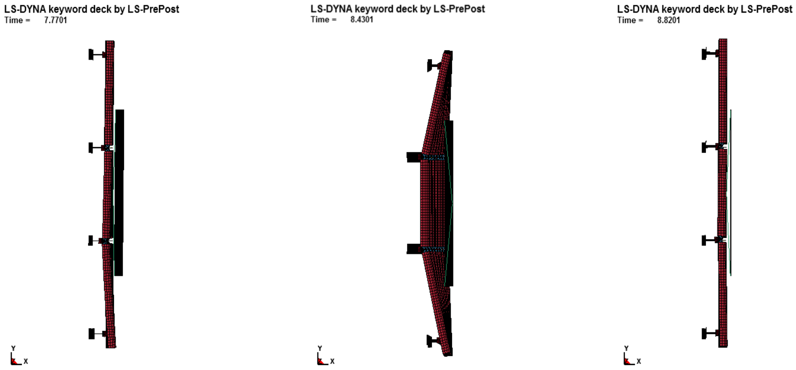

(d) 2nd impact (7.75s~8.82s)

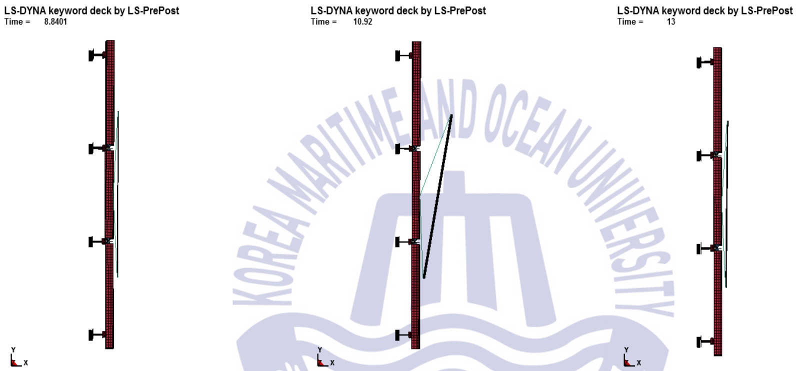

(e) 3rd impact & steady (8.82s~13.00s)

Fig 4.9 Top view of impact simulation behavior of safety barrier and impact medium in Case 1

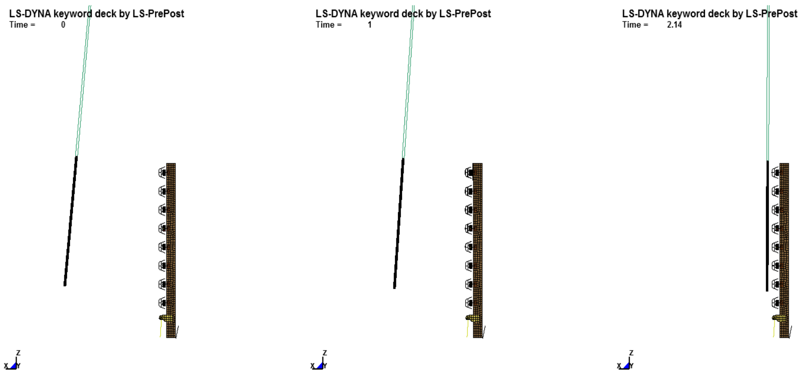

(a) swing to 1st impact (0.00s~2.14s)

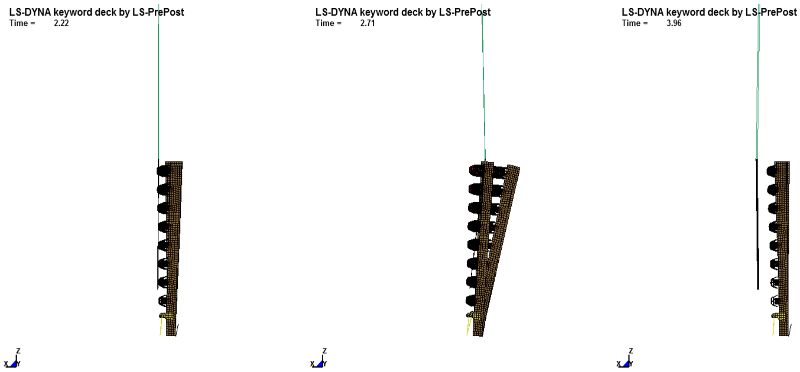

(b) 1st impact (2.14s~3.88s)

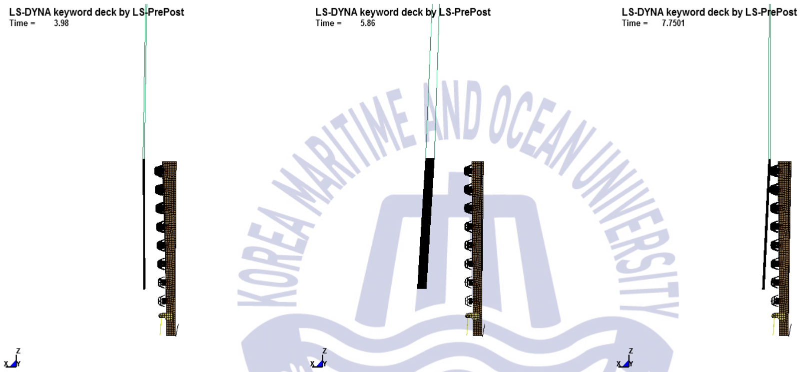

(c) rebounding after 1st impact (3.88s~7.75s)

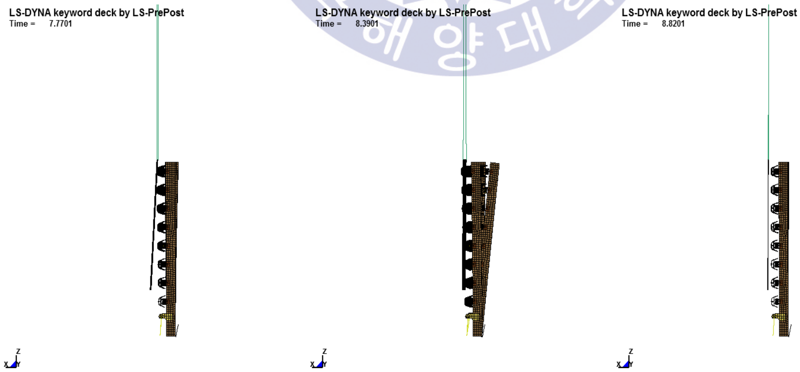

(d) 2nd impact (7.75s~8.82s)

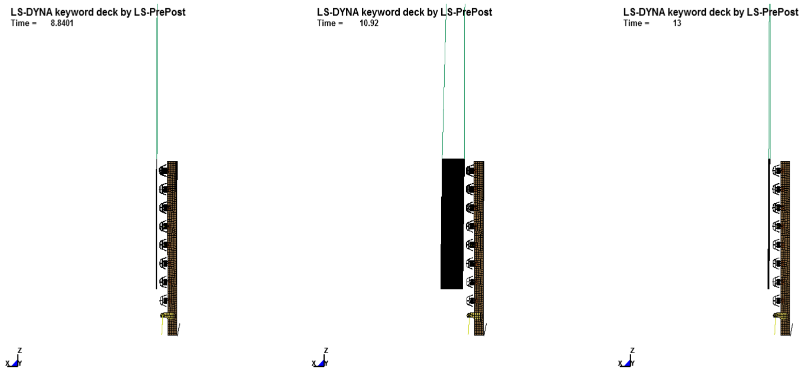

(e) 3rd impact & steady (8.82s~13.00s)

Fig 4.10 Side view of impact simulation behavior of safety barrier and impact medium in Case 1

4.2. Impact simulation of scenarios Case 2 (center, normal height)

Impact simulation of scenario Case 2, as shown in Fig. 3.9, was performed. Impact medium was struck ideally to the safety barrier with normal direction and no rotation, contrary to Case 1 with a little bit rotation to the safety barrier. Figure 4.11 shows its inclined angle responses of Sensors 1~4 in the safety barrier, and their maximum ones at the 1st and 2nd impact peaks are summarized with those of Case 1 in Table 4.2, where their maximum inclined angles were also smaller than the limitation angle 14°, as the scenario of Case 1. Figures 4.12~4.14 illustrate the front, top and side views of the impact simulation behaviors of the safety barrier and impact medium in Case 2. As expected, the inclined angle responses of Sensors 1 & 4 and 2 & 3 were almost the same with each others, contrary to the scenario of Case 1, and the responses in Sensors 1 & 4 in Case 2 were shown a little bit larger than those in scenario Case 1. The impact simulation behaviors of safety barrier and impact medium were almost the same as those of Case 1, except no rotation of impact medium after the rebound of the first and second impact durations.

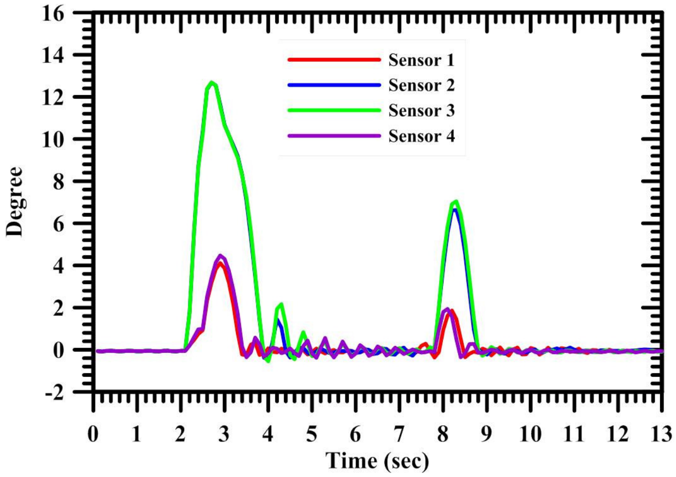

Fig 4.11 Inclined angle responses of Sensors 1~4 in Case 2

Table 4.2 Maximum inclined angles of Sensor 1~4 in Case 2 with those of Case 1

Sensor	Impact peak	Case 2 (°)	Case 1 (°)
1	1st	4.12	4.21
	2nd	1.86	1.51
2	1st	12.68	12.57
	2nd	6.75	6.83
3	1st	12.68	12.68
	2nd	6.76	7.05
4	1st	4.11	3.67
	2nd	1.84	0.93

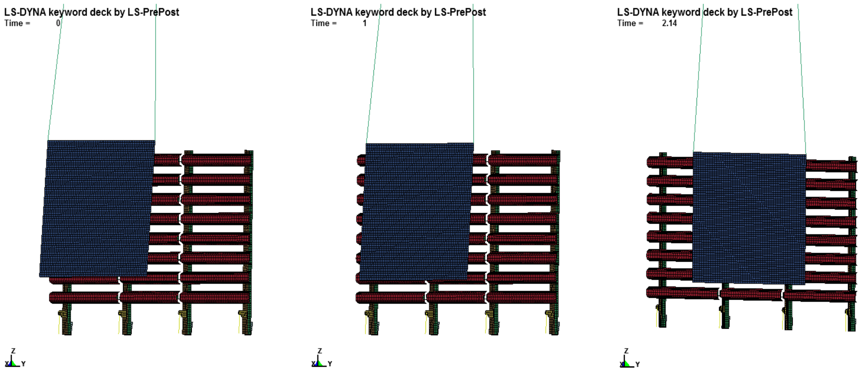

(a) swing to 1st impact (0.00s~2.14s)

(b) 1st impact (2.14s~3.96s)

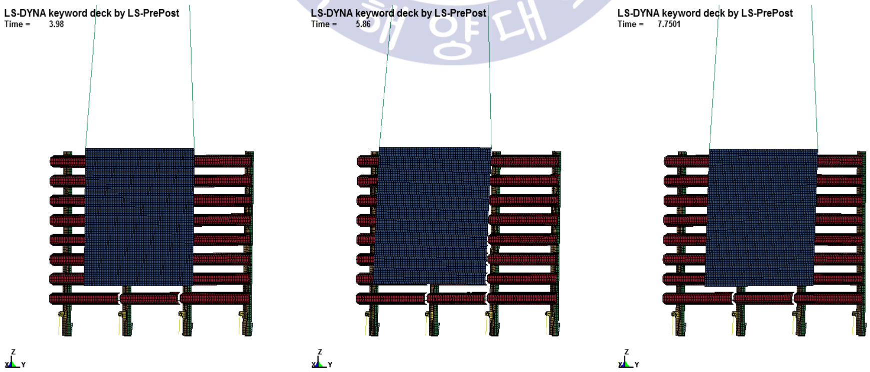

(c) rebounding after 1st impact (3.96s~7.75s)

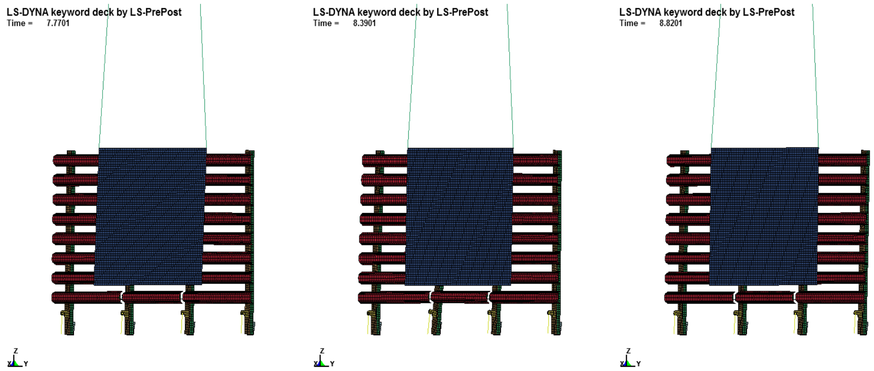

(d) 2nd impact (7.75s~8.82s)

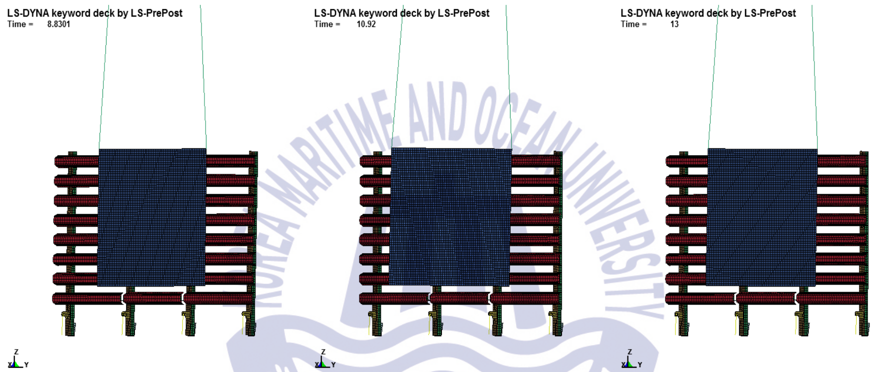

(e) 3rd impact & steady (8.82s~13.00s)

Fig 4.12 Front view of impact simulation behavior of safety barrier and impact medium in Case 2

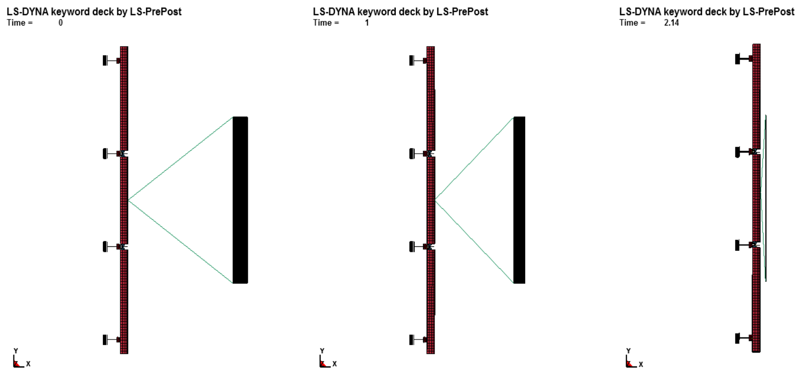

(a) swing to 1st impact (0.00s~2.14s)

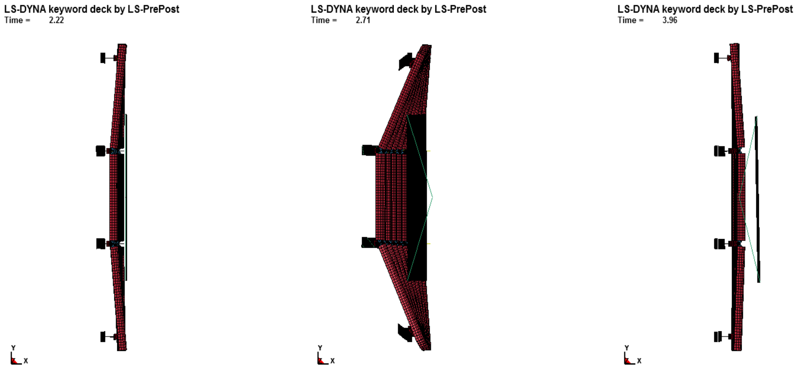

(b) 1st impact (2.14s~3.96s)

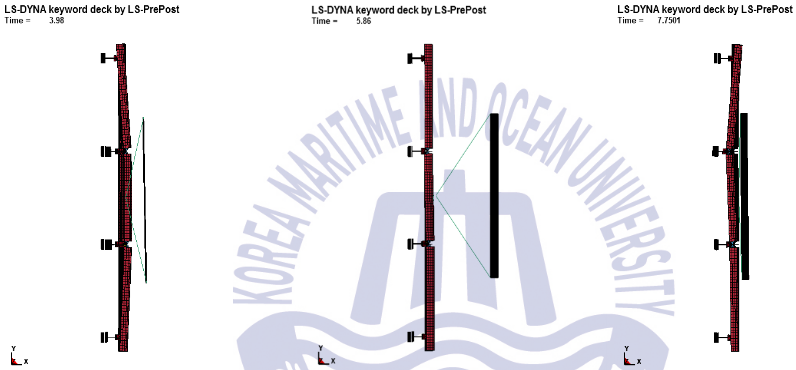

(c) rebounding after 1st impact (3.96s~7.75s)

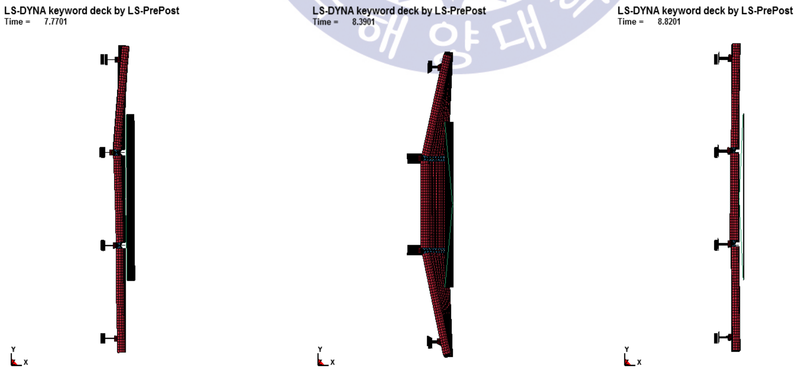

(d) 2nd impact (7.75s~8.82s)

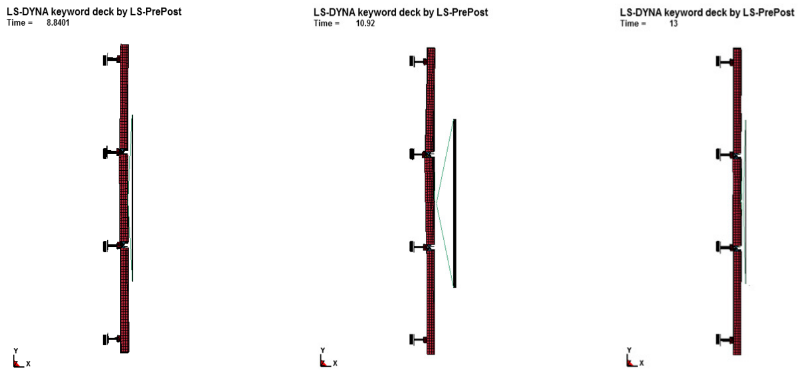

(e) 3rd impact & steady (8.82s~13.0s)

Fig 4.13 Top view of impact simulation behavior of safety barrier and impact medium in Case 2

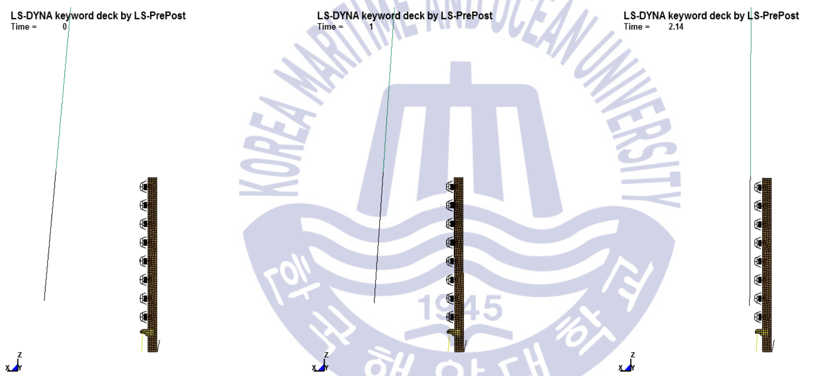

(a) swing to 1st impact (0.00s~2.14s)

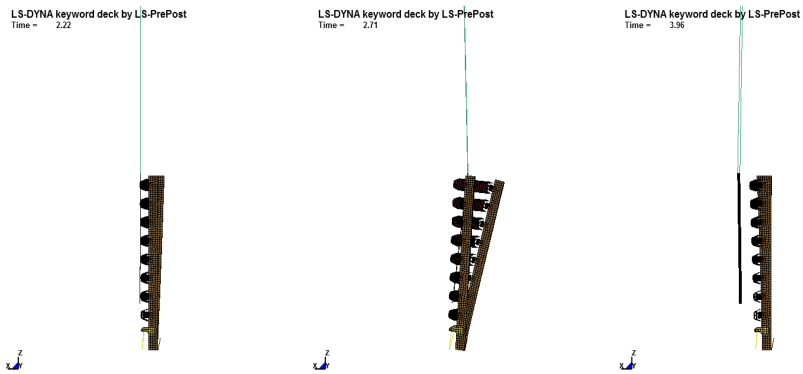

(b) 1st impact (2.14s~3.96s)

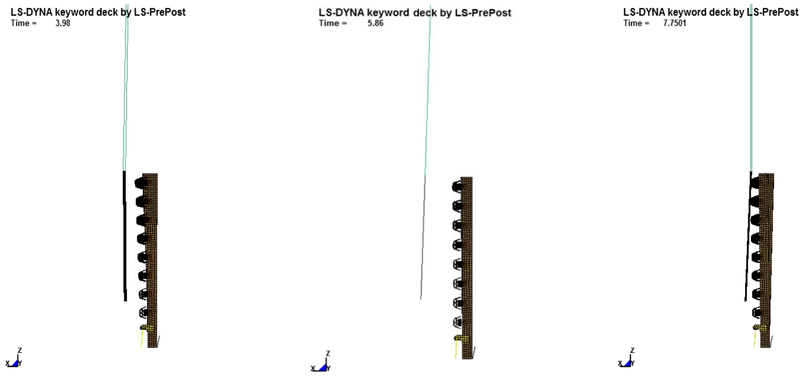

(c) rebounding after 1st impact (3.96s~7.75s)

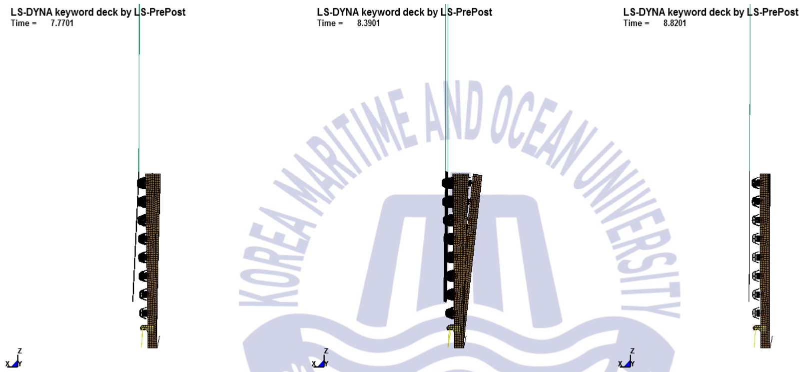

(d) 2nd impact (7.75s~8.82s)

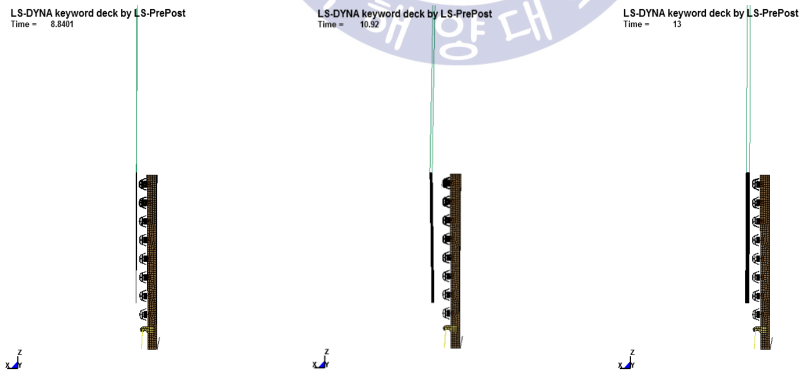

(e) 3rd impact & steady (8.82s~13.00s)

Fig 4.14 Side view of impact simulation behavior of safety barrier and impact medium in Case 2

4.3. Impact simulation of scenarios Case 3 (side, normal height)

Severe impact condition could be expected in the safety barrier from the impact loading positions of impact medium, at the side or/and upper location. In scenario Case 3, as shown in Fig. 3.10, the safety barrier was struck by the impact medium at the right side with normal height. Their inclined angle responses of Sensors 1~4 are illustrated in Fig. 4.15, and their maximum ones at the 1st and 2nd impact peaks are summarized with those of Case 2 in Table 4.3. The front, top and side views of impact simulation behaviors of the safety barrier and impact medium are shown in Figs. 4.16~4.18. As expected, very unsymmetric responses could be found in the Sensors 1 & 2, and no responses, in the Sensors 3 & 4. In the first impact duration, the first column of safety barrier was inclined to the 13.0° around at 2.61sec, and in the second impact duration, the first column, to the 12.3° around at 8.85sec. It could be found that the maximum inclined angles were also smaller than the limitation angle 14°, the same as Cases 1 & 2, and that the impact simulation behaviors of safety barrier and impact medium also demonstrated the side impact characteristics relatively well.

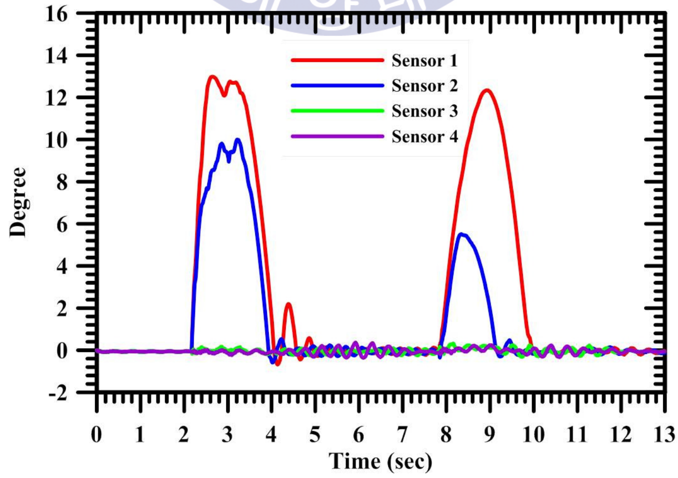

Fig 4.15 Inclined angle responses of Sensors 1~4 in Case 3

Table 4.3 Maximum inclined angles of Sensor 1~4 in Case 3 with those of Case 2

Sensor	Impact peak	Case 3 (°)	Case 2 (°)
1	1st	13.00	4.12
	2nd	12.30	1.86
2	1st	10.00	12.68
	2nd	5.50	6.75
3	1st	0.40	12.68
	2nd	0.40	6.76
4	1st	0.20	4.11
	2nd	0.20	1.84

(a) swing to 1st impact (0.00s~2.14s)

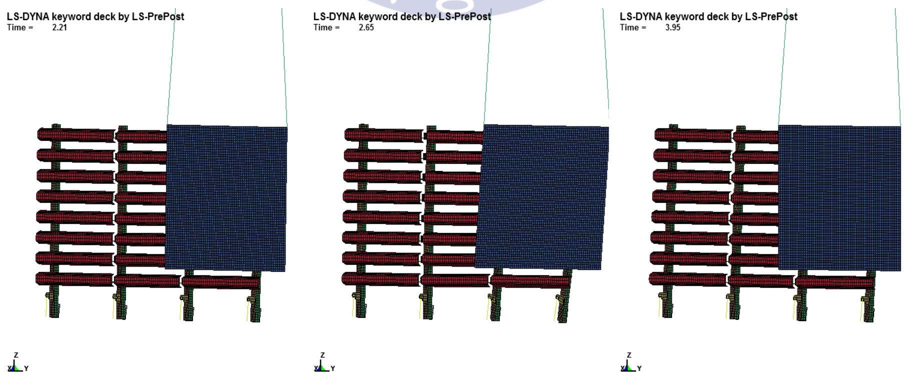

(b) 1st impact (2.14s~3.95s)

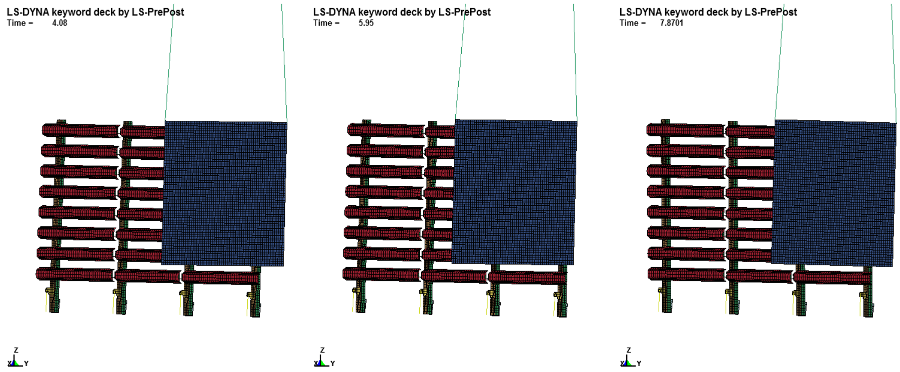

(c) rebounding after 1st impact (3.95s~7.87s)

(d) 2nd impact (7.87s~9.98s)

(e) 3rd impact & steady (9.98s~13.0s)

Fig 4.16 Front view of impact simulation behavior of safety barrier and impact medium in Case 3

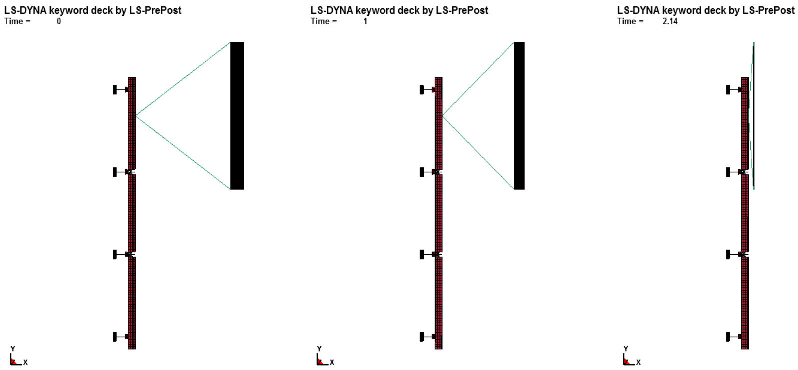

(a) swing to 1st impact (0.00s~2.14s)

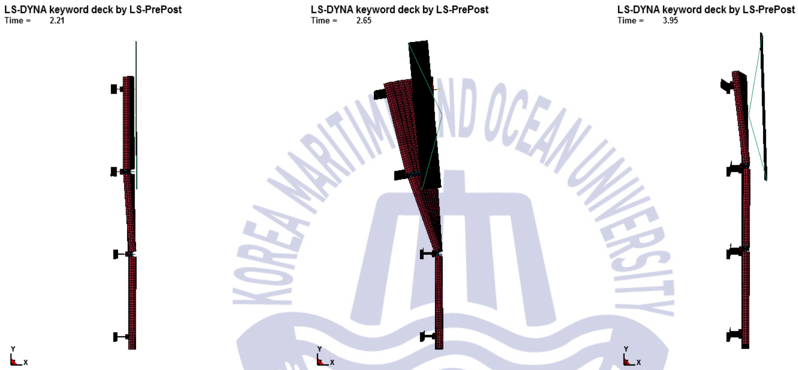

(b) 1st impact (2.14s~3.95s)

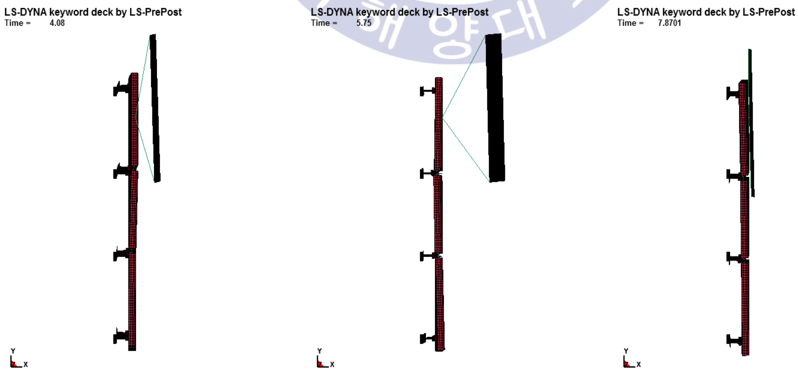

(c) rebounding after 1st impact (3.95s~7.87s)

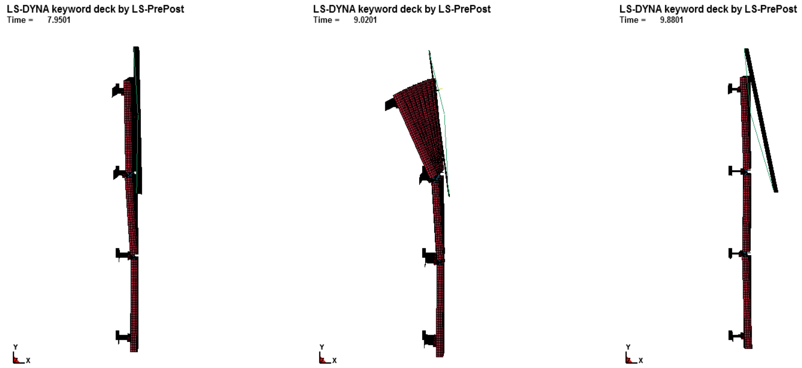

(d) 2nd impact (7.87s~9.98s)

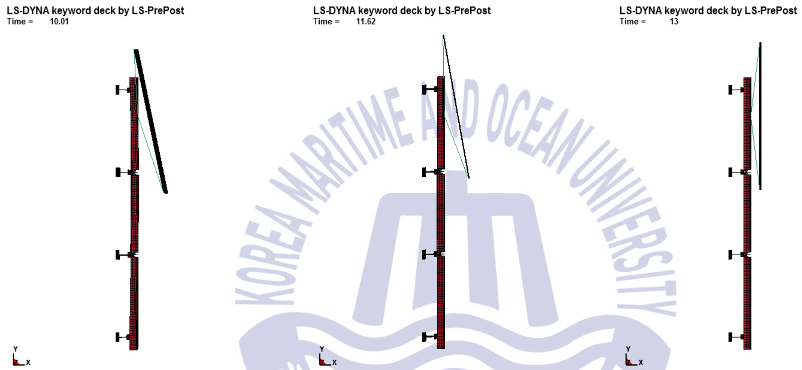

(e) 3rd impact & steady (9.98s~13.0s)

Fig 4.17 Top view of impact simulation behavior of safety barrier and impact medium in Case 3

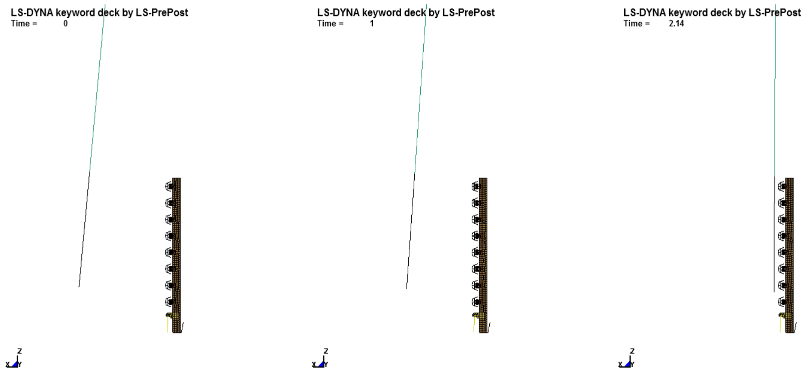

(a) swing to 1st impact (0.00s~2.14s)

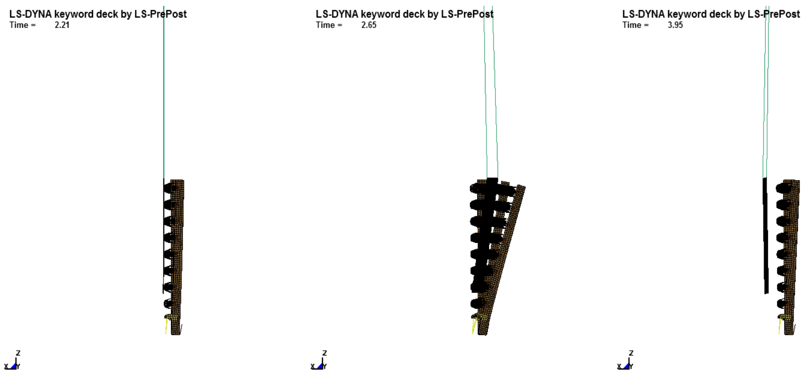

(b) 1st impact (2.14s~3.95s)

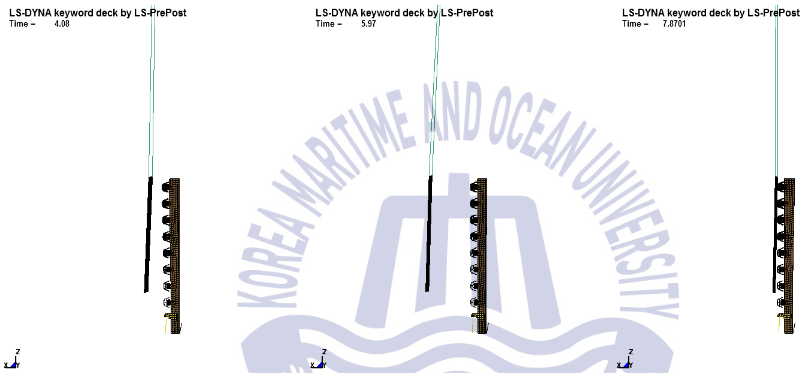

(c) rebounding after 1st impact (3.95s~7.87s)

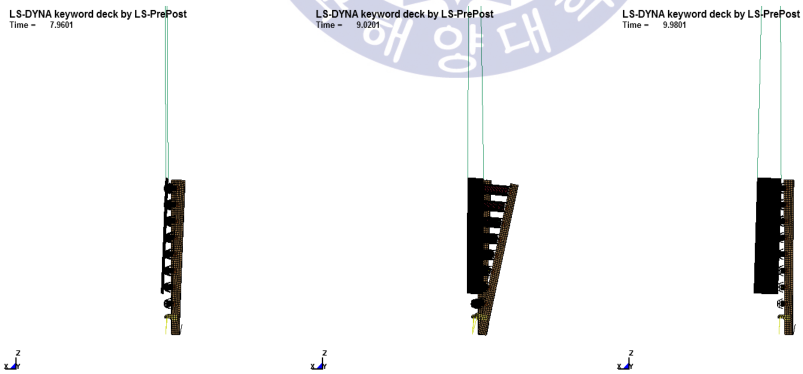

(d) 2nd impact (7.87s~9.98s)

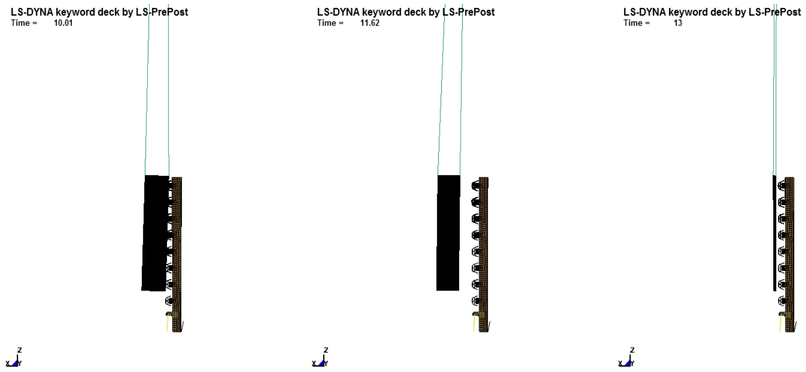

(e) 3rd impact & steady (9.98s~13.0s)

Fig 4.18 Side view of impact simulation behavior of safety barrier and impact medium in Case 3

4.4. Impact simulation of scenarios Case 4 (center, upper height)

In scenario Case 4, as shown in Fig. 3.11, the safety barrier was struck by the impact medium at the center with upper height, as the severe impact condition. Their inclined angle responses of Sensors 1~4 are illustrated in Fig. 4.19, and their maximum ones at the 1st and 2nd impact peaks are summarized with those of Case 4 in Table 4.4. The front, top and side views of impact simulation behaviors of the safety barrier and impact medium, in Figs. 4.20~4.22. As unexpected, the inclined angle responses of Sensors 1~4 were almost the same at the 1st impact duration, where the inclined angles of Sensors 2 & 3 were around 12.68° as the same as those of Cases 2, and those of Sensors 1 & 4, around 12.50° compared to those of 4.12° in Case 2. In the 2nd impact duration, the inclined angles of Sensors 2 & 3 were around 8.53° larger than 6.75° in Case 2, and those of Sensors 1 & 4, around 1.12° smaller than 1.85° in Case 2. The maximum inclined angles were also still smaller than the limitation angle 14°, the same as in Cases 1~3 and test. These response behaviors could be confirmed from the impact simulation behaviors in the safety barrier and impact medium, as shown in Figs. 4.20~4.22.

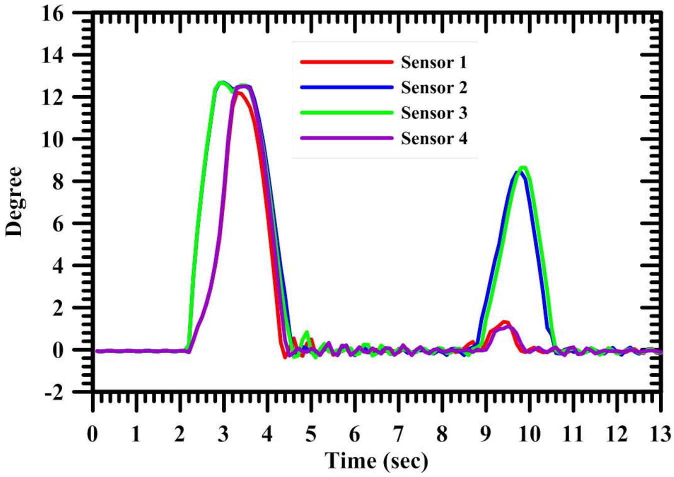

Fig 4.19 Inclined angle responses of safety barrier in Case 4

Table 4.4 Maximum inclined angles of Sensor 1~4 in Case 4 with those of Case 2

Sensor	Impact peak	Case 4 (°)	Case 2 (°)
1	1st	12.47	4.12
	2nd	1.12	1.86
2	1st	12.68	12.68
	2nd	8.52	6.75
3	1st	12.67	12.68
	2nd	8.54	6.76
4	1st	12.50	4.11
	2nd	1.11	1.84

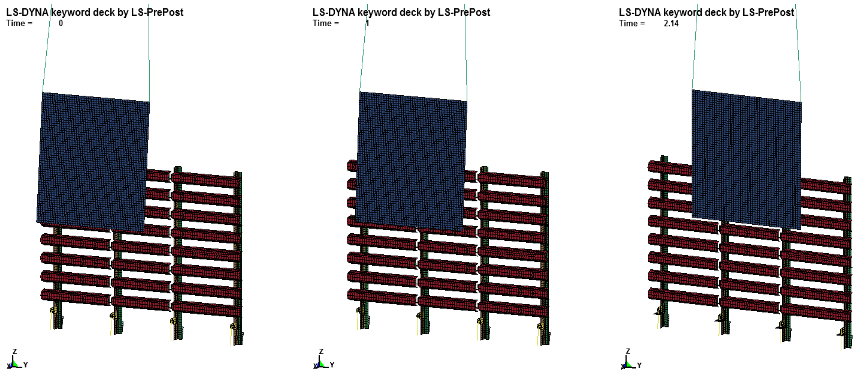

(a) swing to 1st impact (0.00s~2.14s)

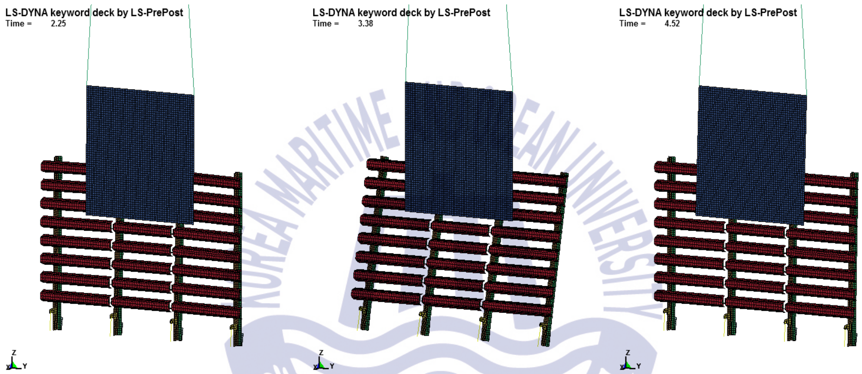

(b) 1st impact (2.14s~4.52s)

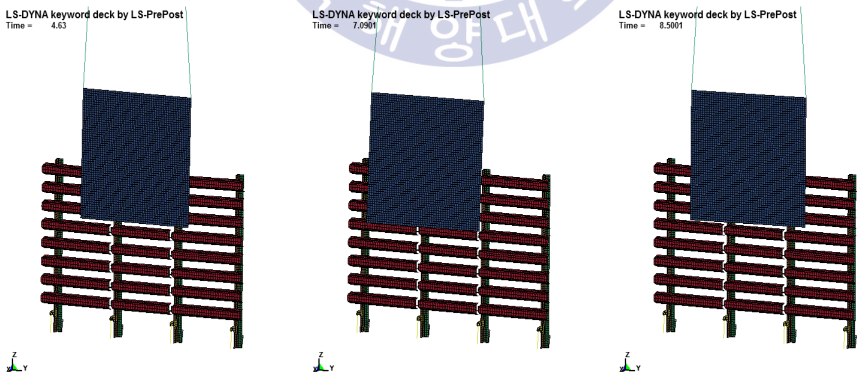

(c) rebounding after 1st impact (4.52s~8.50s)

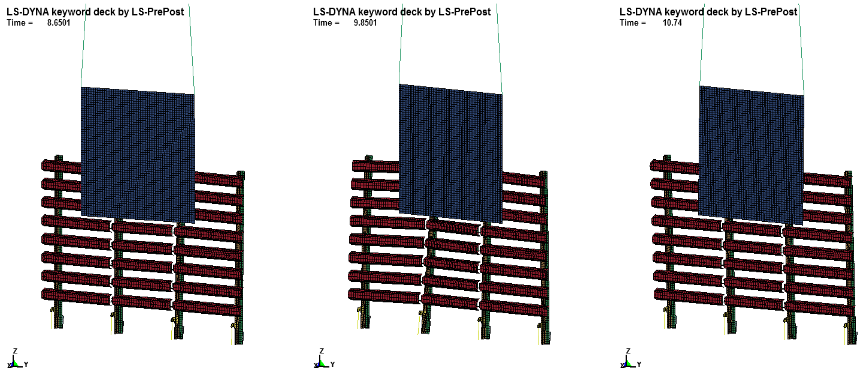

(d) 2nd impact (8.50s~10.74s)

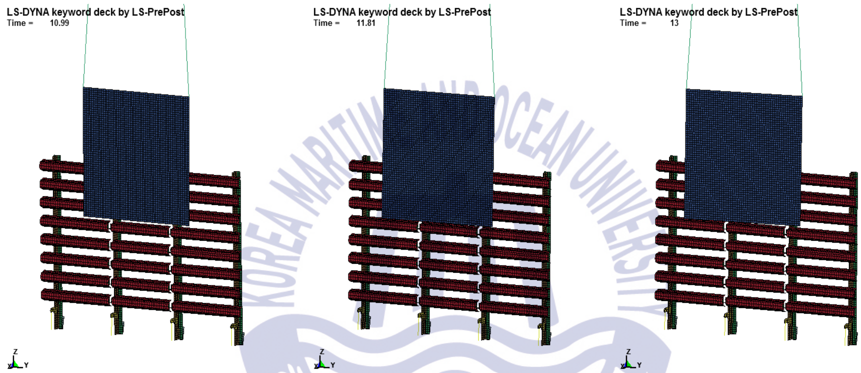

(f) 3rd impact & steady (10.74s~13.00s)

Fig 4.20 Front view of impact simulation behavior of safety barrier and impact medium in Case 4

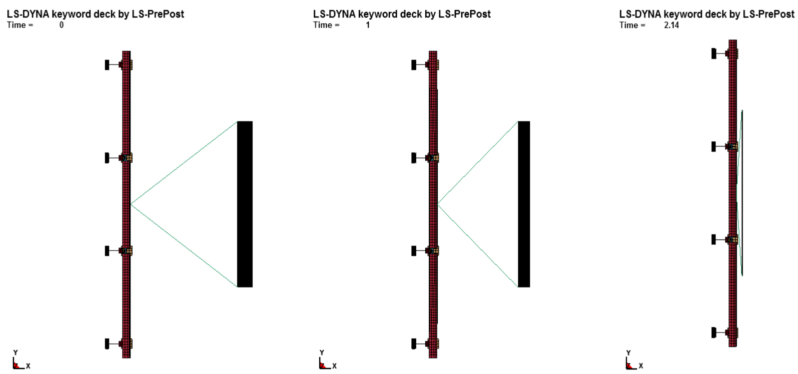

(a) swing to 1st impact (0.00s~2.14s)

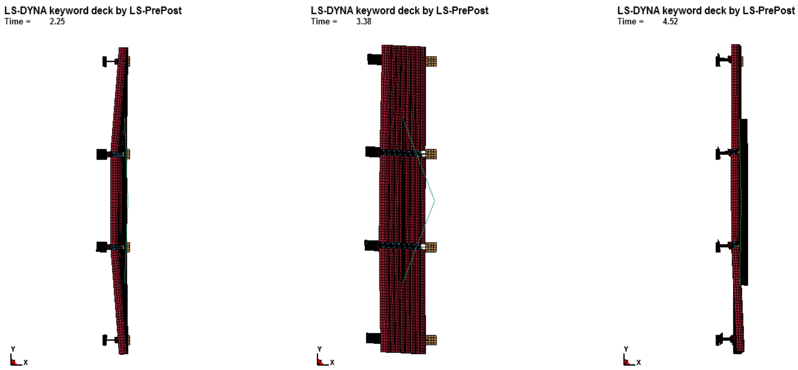

(b) 1st impact (2.14s~4.52s)

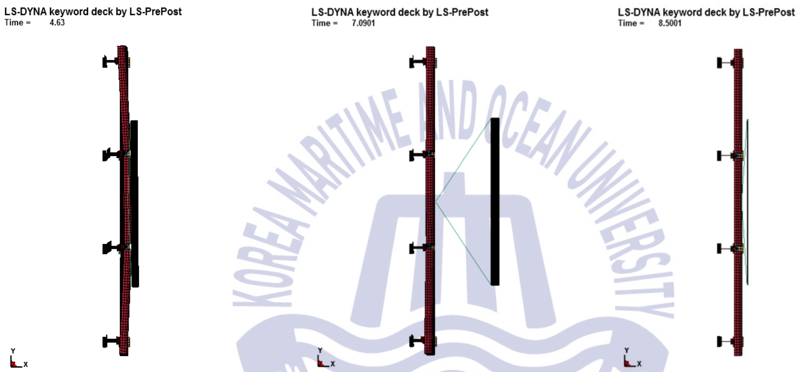

(c) rebounding after 1st impact (4.52s~8.50s)

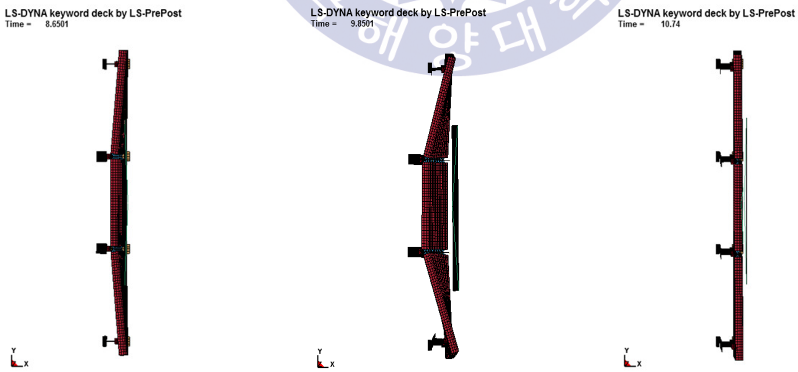

(d) 2nd impact (8.50s~10.74s)

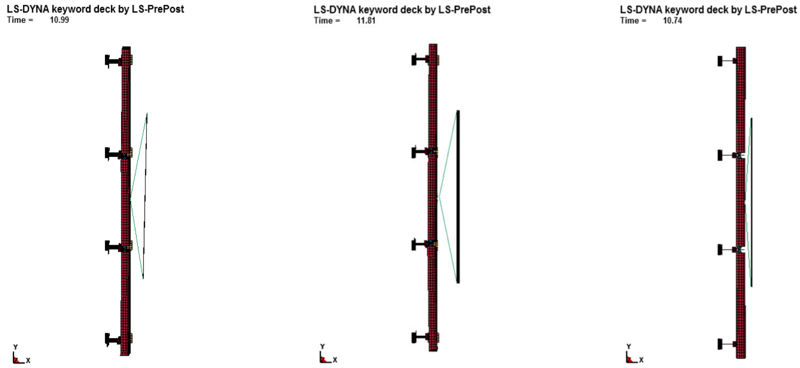

(f) 3rd impact & steady (10.74s~13.00s)

Fig 4.21 Top view of impact simulation behavior of safety barrier and impact medium in Case 4

(a) swing to 1st impact (0.00s~2.14s)

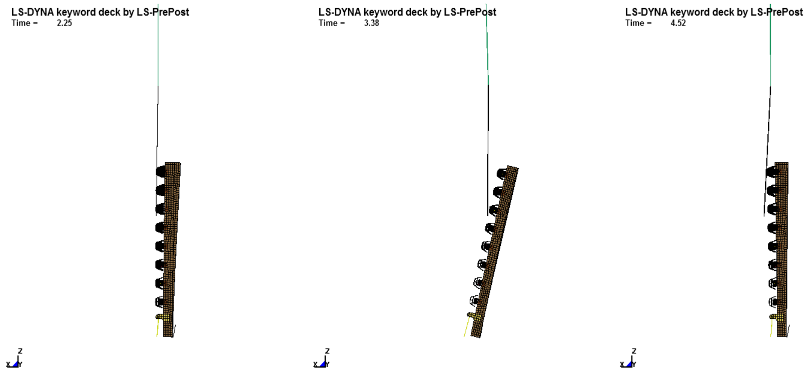

(b) 1st impact (2.14s~4.52s)

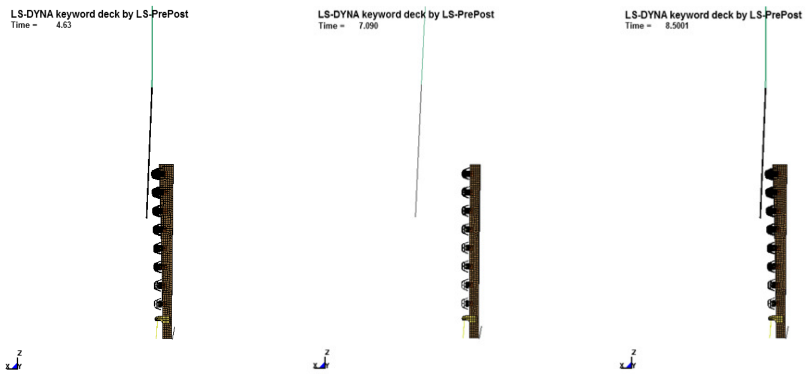

(c) rebounding after 1st impact (4.52s~8.50s)

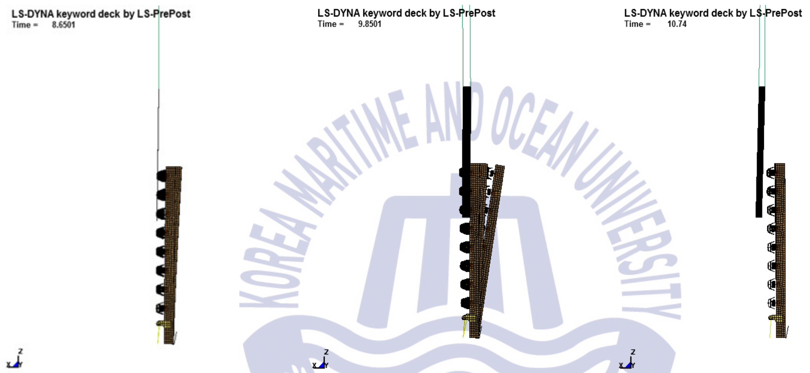

(d) 2nd impact (8.50s~10.74s)

(f) 3rd impact & steady (10.74s~13.00s)

Fig 4.22 Side view of impact simulation behavior of safety barrier and impact medium in Case 4

4.5. Impact simulation of scenarios Case 5 (side, upper height)

Whereas the scenario Case 3 was one of the severe impact conditions as the side impact position with the normal height one compared to Case 2, and Case 4, as the upper height position with the center one compared to Case 2. The scenario Case 5 is the most severe impact condition, such as the side and upper height impact position, as shown in Fig. 3.12, among the scenarios Cases 2~4. Figure 4.23 shows the inclined angle responses of Sensors 1~4 in Case 5. The inclined angle responses of Case 2~5 according to Sensor are shown in Fig. 4.24 for convenient comparison with their responses of the 1st and 2nd impact peaks together at every Sensor, and their maximum inclined angles at the 1st and 2nd impact peaks are summarized in Table 4.5 with those of Cases 2~4. The front, top and side views of impact simulation behaviors of the safety barrier and impact medium are shown in Figs. 4.25~4.27.

As expected, very unsymmetric responses could be found in the Sensors 1 & 2, and no responses, in the Sensors 3 & 4, where these trends were almost the same as Case 3. As the impact position was translated to the upper height position compared to Case 3, the impulse of inclined response angle of the Sensor 1 was increased during the 1st and especially the 2nd impact duration, during the 2nd duration. It could be also found that the maximum inclined angles were also smaller than the limitation angle 14°, the same as Cases 1~4 and test, and that the impact simulation behaviors of safety barrier and impact medium also demonstrated the side and upper height impact characteristics relatively well.

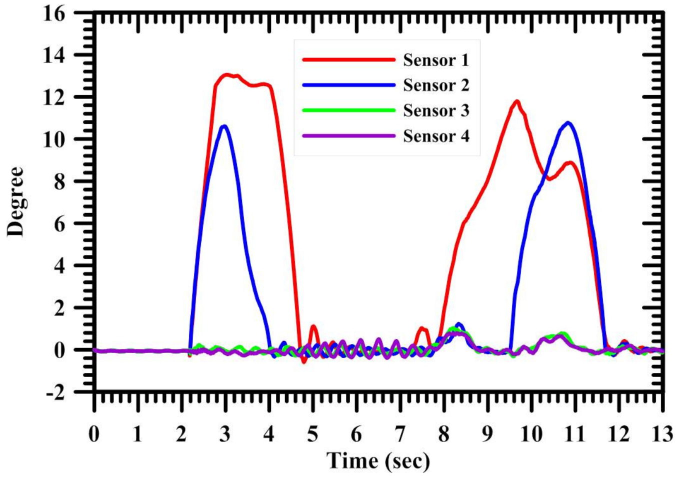

Fig 4.23 Inclined angle responses of safety barrier in Case 5

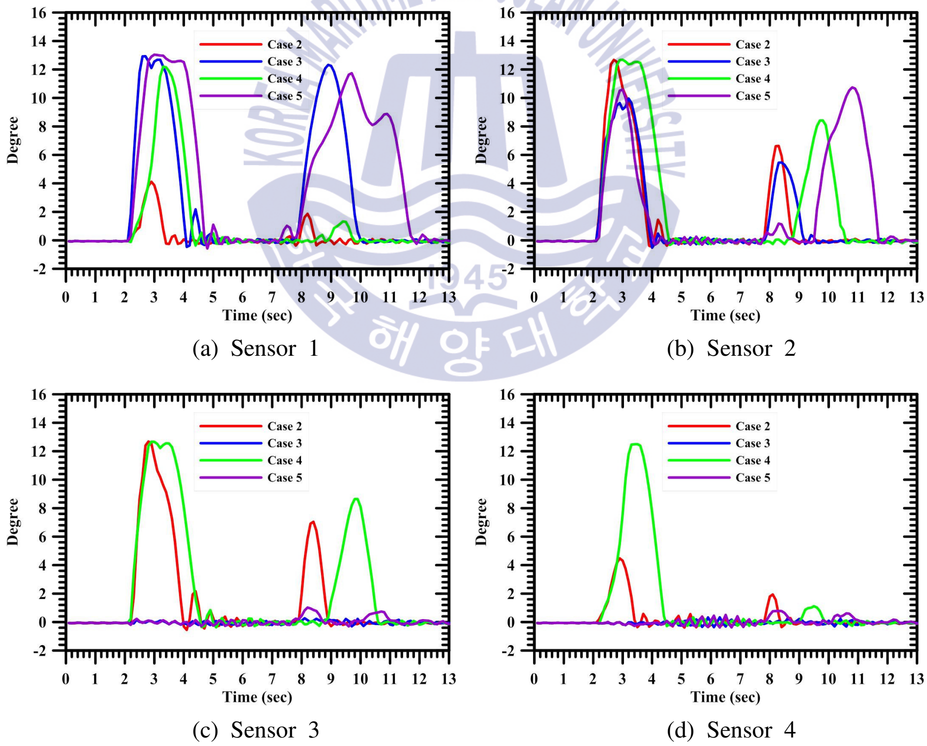

Fig 4.24 Comparison of inclined angle responses of Case 2~5 according to Sensor 1~4

Table 4.5 Maximum inclined angles of Sensor 1~4 in Case 5 with those of Cases 2~4

Sensor	Impact peak	Case 5 (°)	Case 3 (°)	Case 4 (°)	Case 2 (°)
1	1st	13.10	13.00	12.47	4.12
	2nd	11.80	12.30	1.12	1.86
2	1st	10.80	10.00	12.68	12.68
	2nd	10.80	5.50	8.52	6.75
3	1st	0.50	0.40	12.67	12.68
	2nd	0.50	0.40	8.54	6.76
4	1st	0.30	0.20	12.50	4.11
	2nd	0.30	0.20	1.11	1.84

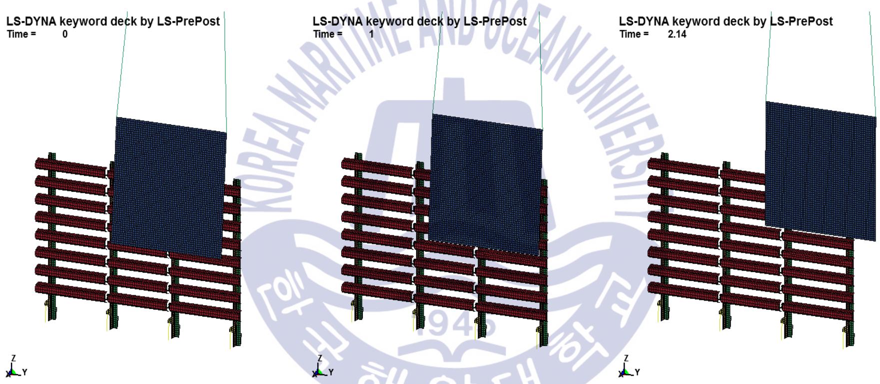

(a) swing to 1st impact (0.00s~2.14s)

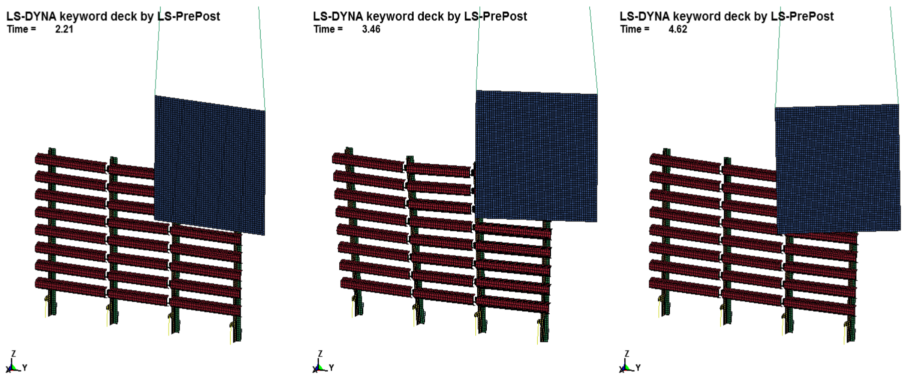

(b) 1st impact (2.14s~4.62s)

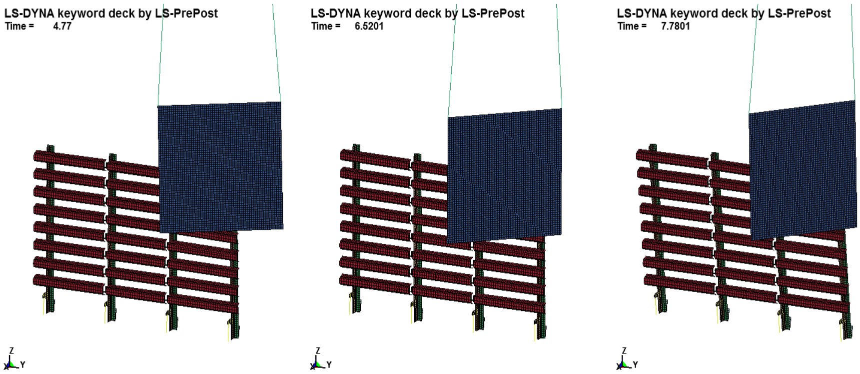

(c) rebounding after 1st impact (4.62s~7.78s)

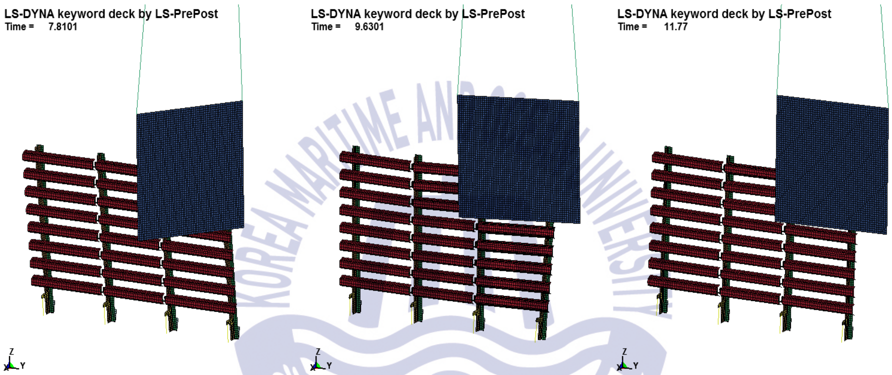

(d) 2nd impact (7.78s~11.77s)

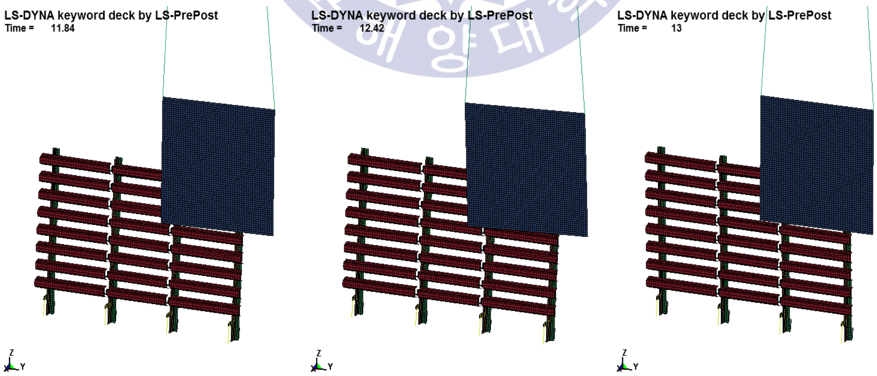

(e) 3rd impact & steady (11.77s~13.00s)

Fig 4.25 Front view of impact simulation behavior of safety barrier and impact medium in Case 5

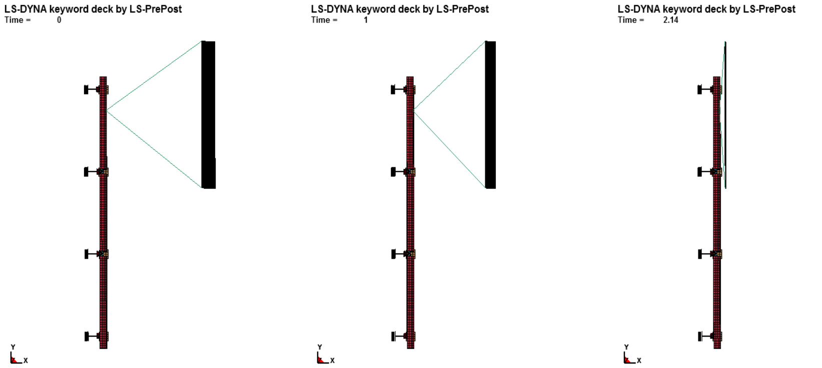

(a) swing to 1st impact (0.00s~2.14s)

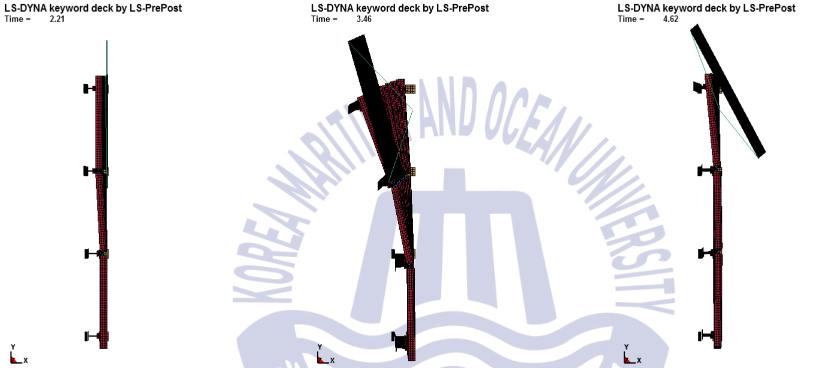

(b) 1st impact (2.14s~4.62s)

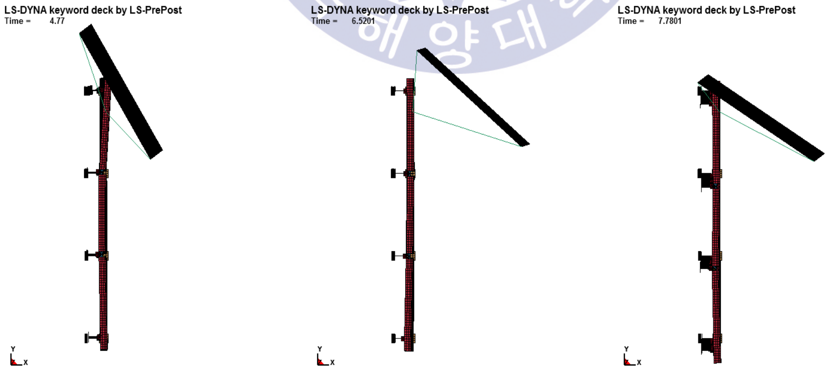

(c) rebounding after 1st impact (4.62s~7.78s)

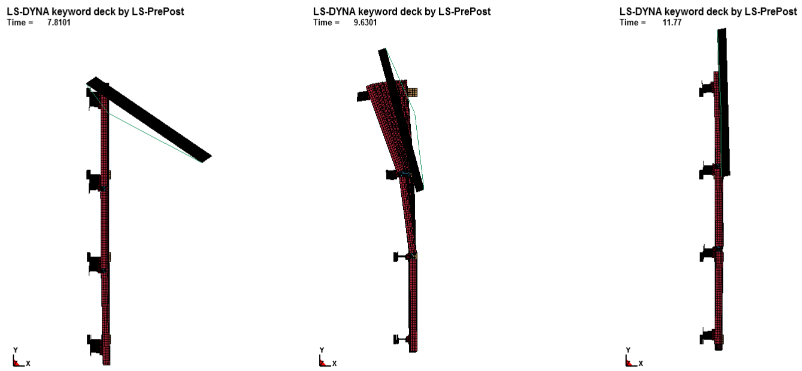

(d) 2nd impact (7.78s~11.77s)

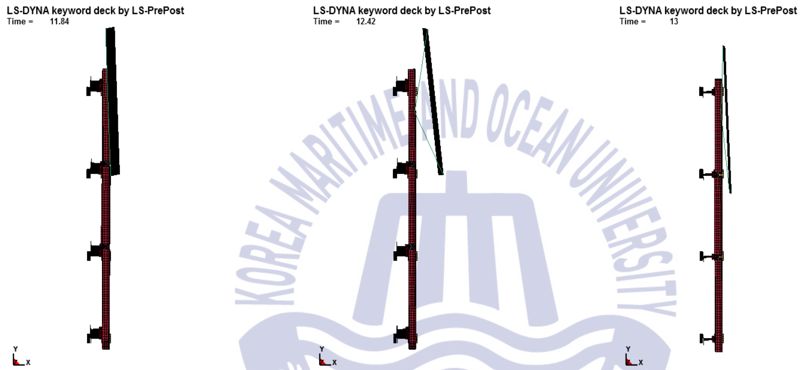

(e) 3rd impact & steady (11.77s~13.00s)

Fig 4.26 Top view of impact simulation behavior of safety barrier and impact medium in Case 5

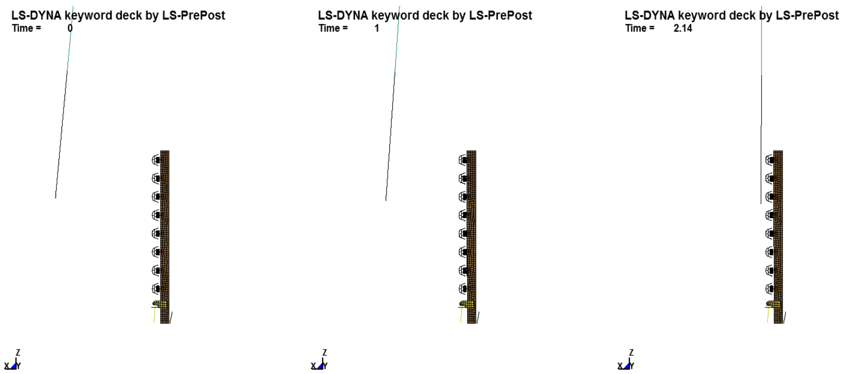

(a) swing to 1st impact (0.00s~2.14s)

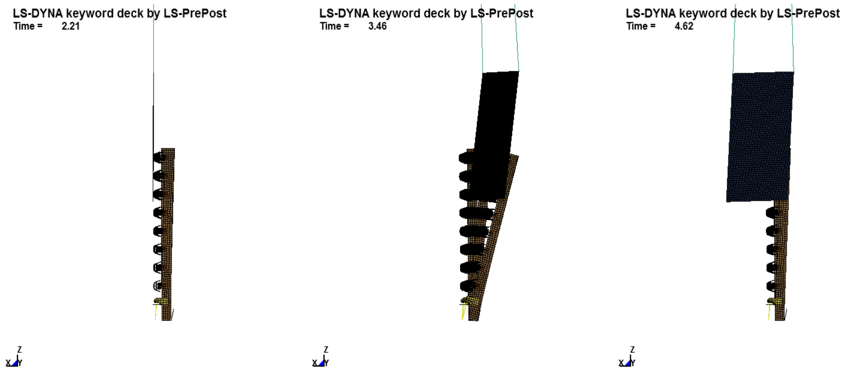

(b) 1st impact (2.14s~4.62s)

(c) rebounding after 1st impact (4.62s~7.78s)

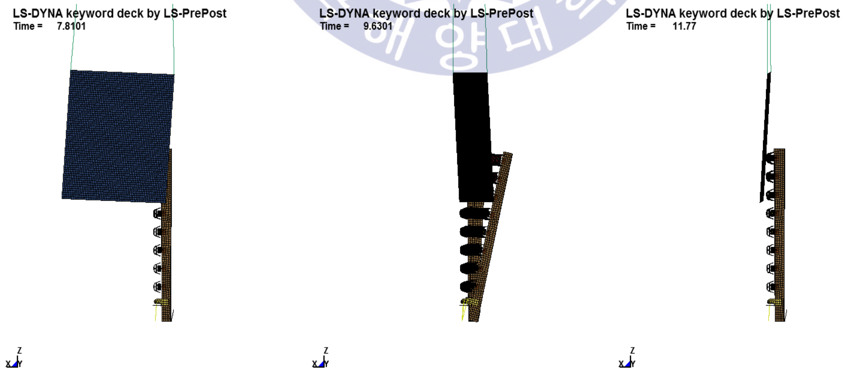

(d) 2nd impact (7.78s~11.77s)

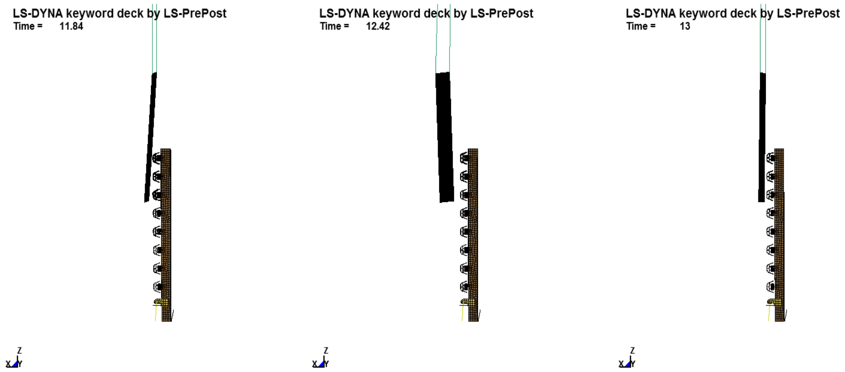

(e) 3rd impact & steady (11.77s~13.00s)

Fig 4.27 Side view of impact simulation behavior of safety barrier and impact medium in Case 5

5. Structural Safety Assessment of Safety Barrier

Structural safety assessment of safety barrier were carried out by the local assessment of the maximum stress in its components, such as guide rails and columns, in Cases 1~5. Although no damage of safety barrier was already found in the impact test, the location of maximum von Mises effective stress should be figured out for the maintenance. Since this impact accident to the safety barrier could be expected repeatedly, it is necessary to predict and protect the possible impact damages including the fatigue failure through the structural safety assessment. The strength evaluation was also conducted in the springs of hydraulic spring-damper absorber, and their tension deformation should be under the 55.0mm, as shown in Force-Stroke curve of spring in hydraulic spring-damper absorber in Fig. 3.7 (SEBOTECH, 2016), for the protection of damage and for the security of its restoration. Tables 5.1 & 5.2 summarize the maximum von Mises effective stress and deformation results of scenario Cases 1~5.

Table 5.1 Strength evaluation of each component of safety barrier according to scenario (unit : MPa)

Scenario	impact	guide rail	column	reference Von-mises stress (British Standard, 2007)
Case 1	1st	17.9	21.9	260
	2nd	5.0	16.8	
Case 2	1st	11.7	27.4	260
	2nd	4.5	16.4	
Case 3	1st	17.7	51.1	260
	2nd	4.5	23.3	
Case 4	1st	15.0	26.2	260
	2nd	5.0	13.5	
Case 5	1st	13.3	98.8	260
	2nd	5.3	27.1	

Table 5.2 Strength evaluation of hydraulic spring absorber of safety barrier according to scenario (unit : mm)

Scenario	impact	hydraulic absorber	reference deformation (SEBOTECH, 2016)
Case 1	1st	38.5	55
	2nd	23.2	
Case 2	1st	38.6	55
	2nd	23.2	
Case 3	1st	40.8	55
	2nd	35.5	
Case 4	1st	38.6	55
	2nd	27.3	
Case 5	1st	41.4	55
	2nd	35.4	

5.1 Structural safety assessment of Case 1 (impact test condition)

In the structural safety assessment of Case 1, the von Mises effective stress distributions of guide rails and columns are shown in Fig. 5.1, where their locations of the maximum von Mises effective stresses in its components are also marked by red circles. The maximum von Mises effective stresses of guide rails and columns were 17.9MPa and 21.8MPa in 1st impact and 5.0MPa and 16.8MPa in 2nd impact, respectively, as shown in Table 5.1. The spring deformations of Sensor 1~4 in hydraulic spring-damper absorber are shown in Fig. 5.2, where almost the same response trends could be found as the those of inclined angle response, as shown in Fig. 4.7, and their maximum spring deformations of Sensors 3 & 2 were 38.5mm and 23.2mm in 1st and 2nd impact peaks, as shown in Table 5.2. It could be found that no plastic deformation occurred as the impact test, such as very low maximum elastic von Mises effective stresses in the guide rails and columns, and the maximum spring deformation under the limit 55.0mm. Therefore, it could be said that the safety barrier could be sufficiently safe in the structural safety assessment of Case 1.

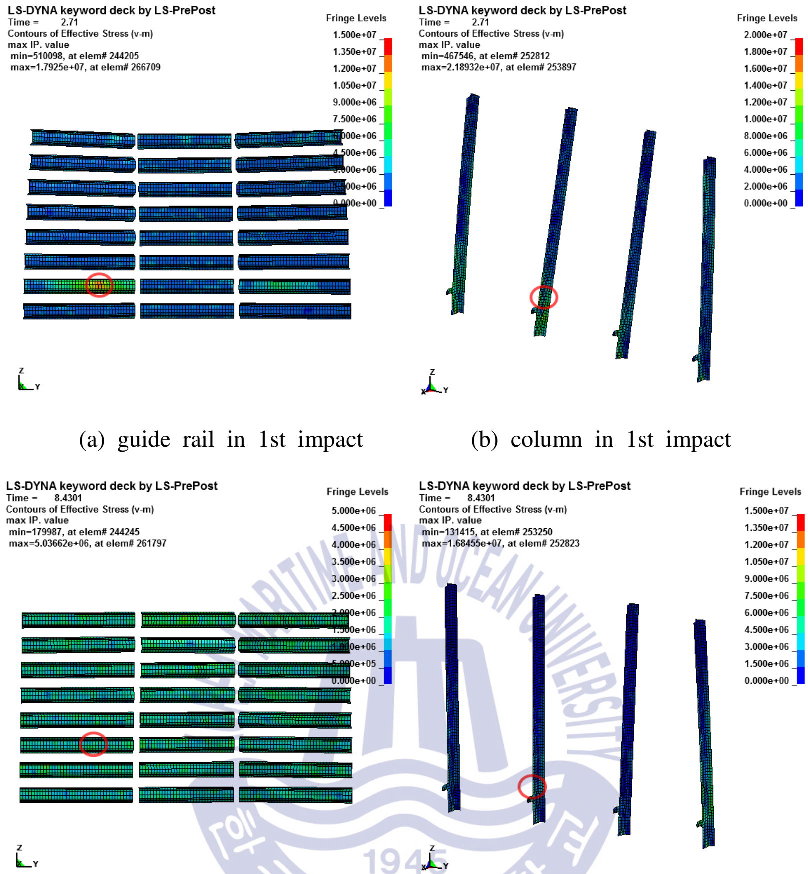

(a) guide rail in 1st impact (b) column in 1st impact

(c) guide rail in 2nd impact (d) column in 2nd impact

Fig 5.1 von Mises effective stress distributions of guide rails and columns of safety barrier in Case 1

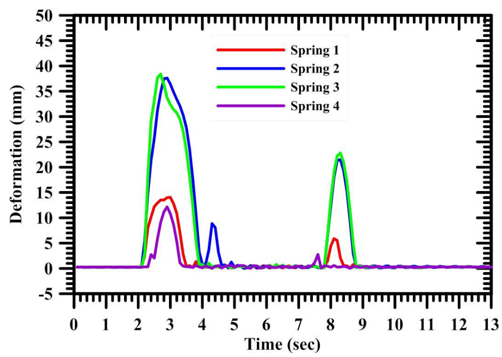

Fig 5.2 Deformation response of spring in hydraulic absorber in Case 1

5.2 Structural safety assessment of Case 2 (center, normal height)

In the structural safety assessment of Case 2, Fig. 5.3 shows the von Mises effective stress distributions of guide rails and columns. The maximum von Mises effective stresses of guide rails and columns were 11.7MPa and 27.4MPa in 1st impact and 4.5MPa and 16.4MPa in 2nd impact, respectively, as shown in Table 5.1. The spring deformations of Sensors 1~4 in hydraulic spring-damper absorber are shown in Fig. 5.4, where almost the same response trends could be found as the those of inclined angle response, as shown in Fig. 4.11, as Case 1, and their maximum spring deformations of Sensors 2 & 3 were 38.6mm and 23.2mm in 1st and 2nd impact peaks, as shown in Table 5.2. It could be found that the maximum von Mises effective stresses in the 7th guide rails and the 2nd & 3rd columns and the maximum deformation in the springs of Sensors 2 & 3 occurred relatively symmetrically contrary to Case 1, and that the maximum deformations in the 1st & 2nd impact peaks in Case 2 were almost the same as those in Case 1. Whereas the maximum stress in the guide rail in Case 2 was smaller than that of Case 1, that of column in Case 2, than that of Case 1. There was no plastic deformation as Case 1, such as very low maximum elastic von Mises effective stresses in the guide rails and columns, and the maximum spring deformation under the limit 55.0mm. Therefore, it could be also said that the safety barrier would have sufficient structural strength in Case 2.

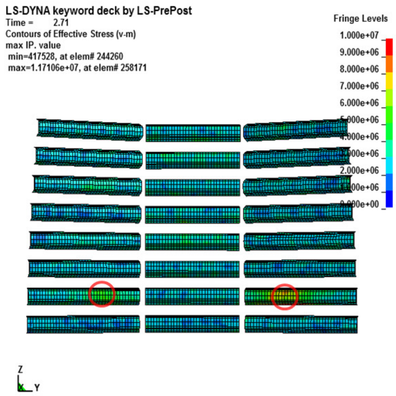

(a) guide rail in 1st impact

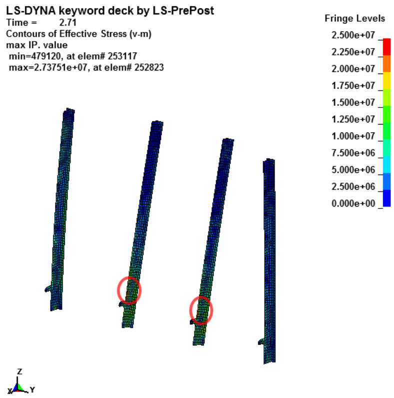

(b) column in 1st impact

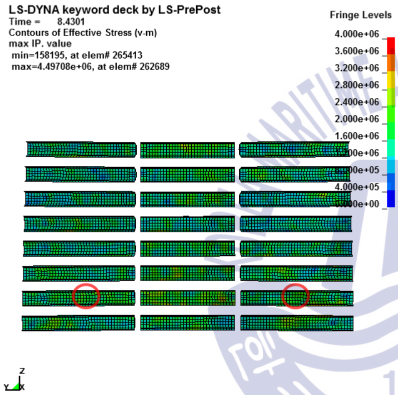

(c) guide rail in 2nd impact

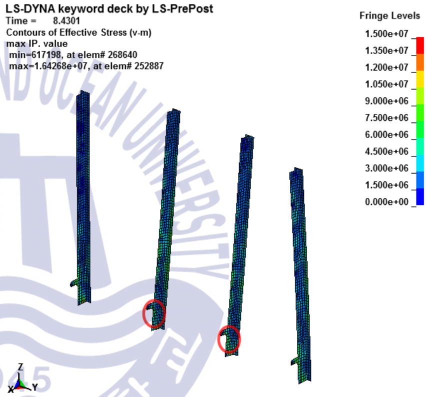

(d) column in 2nd impact

Fig 5.3 von Mises effective stress distributions of guide rails and columns of safety barrier in Case 2

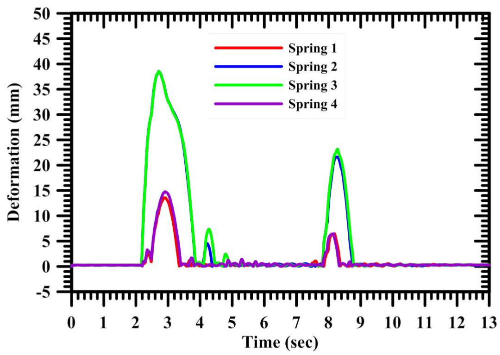

Fig 5.4 Deformation response of spring in hydraulic absorber in Case 2

5.3 Structural safety assessment of Case 3 (side, normal height)

In the structural safety assessment of Case 3, Fig. 5.5 shows the von Mises effective stress distributions of guide rails and columns. The maximum von Mises effective stresses of guide rails and columns were 17.7MPa and 51.1MPa in 1st impact and 4.5MPa and 23.3MPa in 2nd impact, respectively, as shown in Table 5.1. The spring deformations of Sensors 1~4 in hydraulic spring-damper absorber are shown in Fig. 5.6, where almost the same response trends could be found as the those of inclined angle response, as shown in Fig. 4.15, as Cases 1 & 2, and their maximum spring deformations of Sensor 1 were 40.8mm and 35.5mm in 1st and 2nd impact peaks, as shown in Table 5.2. It could be found that the maximum von Mises effective stresses in the 7th guide rail close to Sensor 1 and the 1st column and the maximum deformation in the spring of Sensors 1 occurred unsymmetrically contrary to Cases 1 & 2, and that the maximum deformations in the 1st & 2nd impact peaks in Case 3 were a little larger and much more larger than those in Case 2, respectively. Whereas the maximum stress in the guide rail was almost the same as Case 1, that of 1st column in Case 3, much larger than that of Case 2. There was also no plastic deformation as Cases 1 & 2, such as low maximum elastic von Mises effective stresses in the 1st column, and the maximum spring deformation still under the limit 55.0mm. Therefore, it could be also said that the safety barrier would have sufficient structural strength in Case 3.

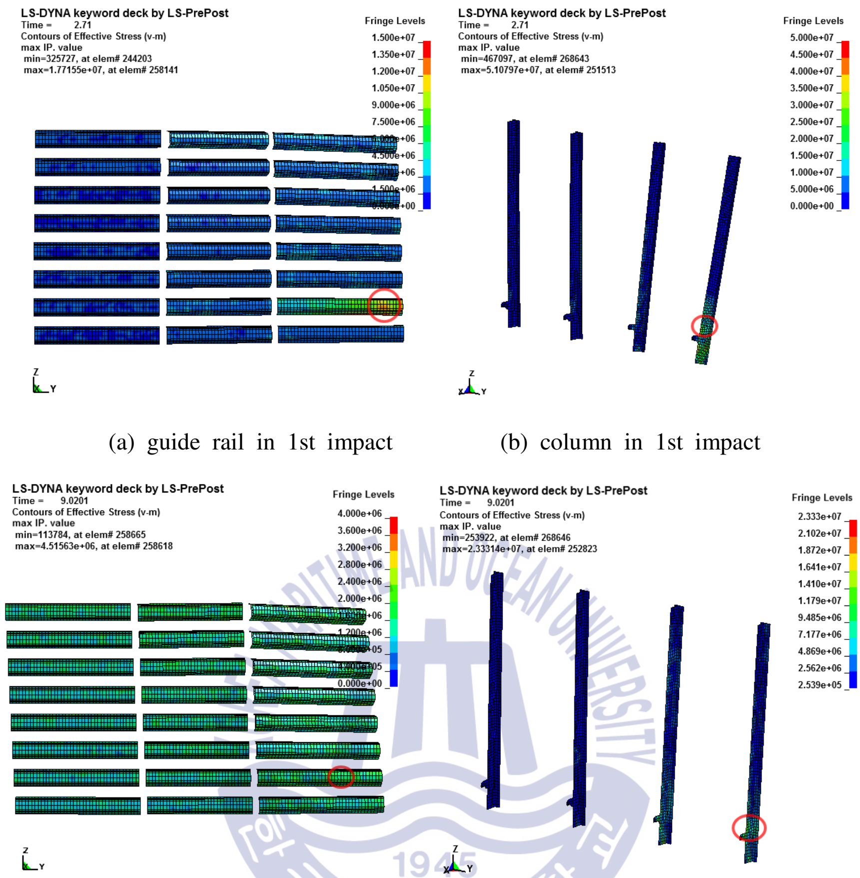

(a) guide rail in 1st impact (b) column in 1st impact

(c) guide rail in 2nd impact (d) column in 2nd impact

Fig 5.5 von Mises effective stress distributions of guide rails and columns of safety barrier in Case 3

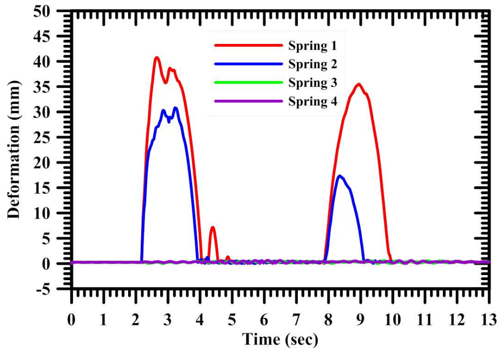

Fig 5.6 Deformation response of spring in hydraulic absorber in Case 3

5.4 Structural safety assessment of Case 4 (center, upper height)

In the structural safety assessment of Case 4, Fig. 5.7 shows the von Mises effective stress distributions of guide rails and columns. The maximum von Mises effective stresses of guide rails and columns were 15.0MPa and 26.2MPa in 1st impact and 5.0MPa and 13.5MPa in 2nd impact, respectively, as shown in Table 5.1. The spring deformations of Sensors 1~4 in hydraulic spring-damper absorber are shown in Fig. 5.8, where almost the same response trends could be found as the those of inclined angle response, as shown in Fig. 4.15, as Cases 1~3, and their maximum spring deformations of Sensors 2 & 3 were 38.6mm and 27.3mm in 1st and 2nd impact peaks, as shown in Table 5.2. It could be found that the maximum von Mises effective stresses in the 3rd guide rails and the 2nd & 3rd columns and the maximum deformation in the springs of Sensors 2 & 3 occurred relatively symmetrically as Case 2, and that the maximum deformations in the 1st & 2nd impact peaks in Case 4 were almost the same as those in Cases 1 & 2. Whereas the maximum stress in the guide rail in Case 4 was smaller than that of Case 2, that of column in Case 2, almost the same as that of Case 2. There was no plastic deformation as Cases 1~3, such as very low maximum elastic von Mises effective stresses in the guide rails and columns, and the maximum spring deformation under the limit 55.0mm. Therefore, it could be also said that the safety barrier would have sufficient structural strength in the Case 4.

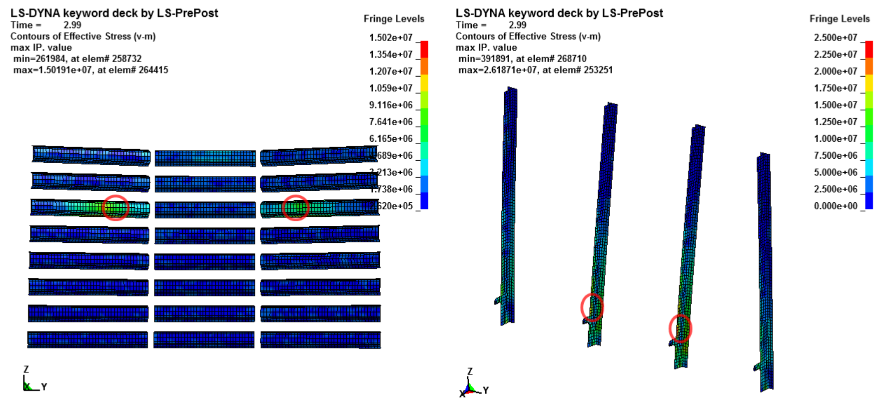

(a) guide rail in 1st impact　　(b) column in 1st impact

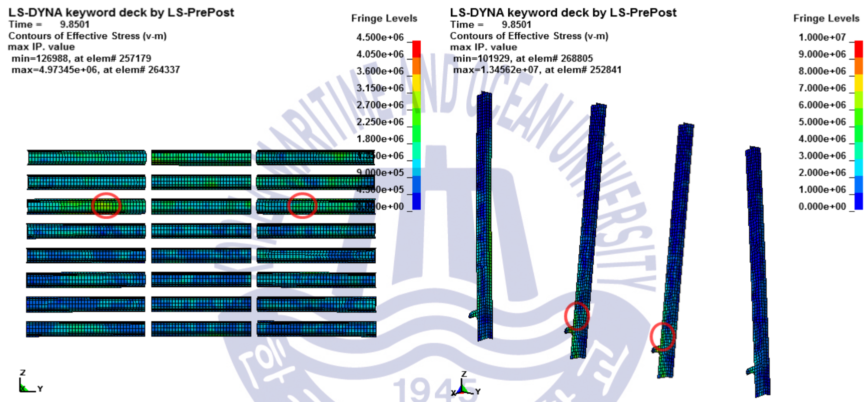

(c) guide rail in 2nd impact　　(d) column in 2nd impact

Fig 5.7 von Mises effective stress distributions of guide rails and columns of safety barrier in Case 4

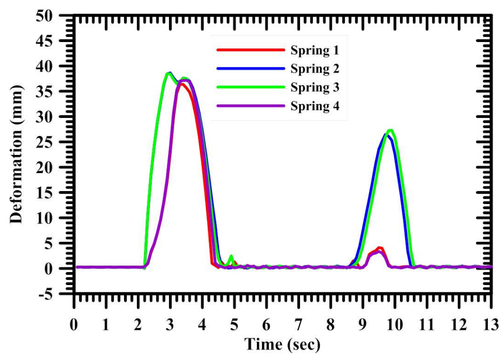

Fig 5.8 Deformation response of spring in hydraulic absorber in Case 4

5.5 Structural safety assessment of Case 5 (side, upper height)

In the structural safety assessment of Case 5, Fig. 5.9 shows the von Mises effective stress distributions of guide rails and columns. The maximum von Mises effective stresses of guide rails and columns were 13.3MPa and 98.8MPa in 1st impact and 5.3MPa and 27.1MPa in 2nd impact, respectively, as shown in Table 5.1. The spring deformations of Sensors 1~4 in hydraulic spring-damper absorber are shown in Fig. 5.10, where almost the same response trends could be found as the those of inclined angle response, as shown in Fig. 4.15, as Cases 1~4, and their maximum spring deformations of Sensor 1 were 41.4mm and 35.4mm in 1st and 2nd impact peaks, as shown in Table 5.2. It could be found that the maximum von Mises effective stresses in the 3rd guide rails and the 1st column and the maximum deformation in the spring of Sensors 1 occurred relatively unsymmetrically as Case 3, and that the maximum deformations in the 1st & 2nd impact peaks in Case 5 were almost the same as those in Case 3. The maximum deformation in the 1st spring of hydraulic absorber in Case 5 was very larger in the all Cases, due to the largest impulse of unsymmetric impact loading, as the inclined angle response of the Sensor 1. There was still no plastic deformation as the Cases 1~4, even though the maximum von Mises effective stress 98.8MPa occurred at the 1st column, and the maximum spring deformation under the limit 55.0mm. Therefore, it could be also said that the safety barrier would have sufficient structural strength in Case 5, however, attention and inspection would be required in the severe impact loading case, such as Case 5.

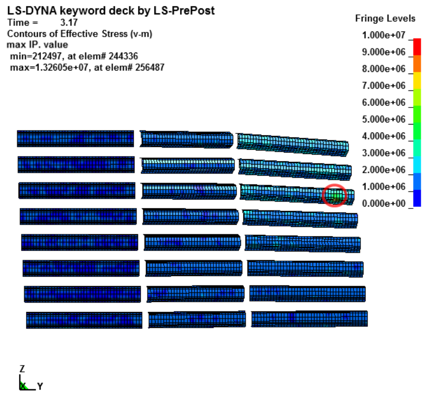

(a) guide rail in 1st impact

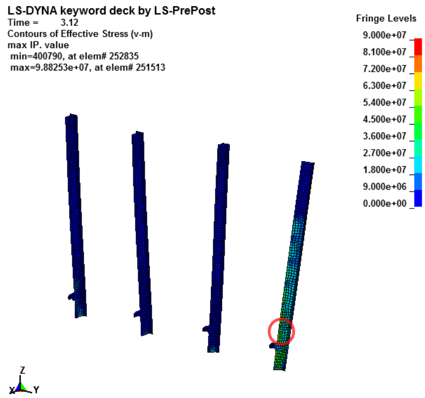

(b) column in 1st impact

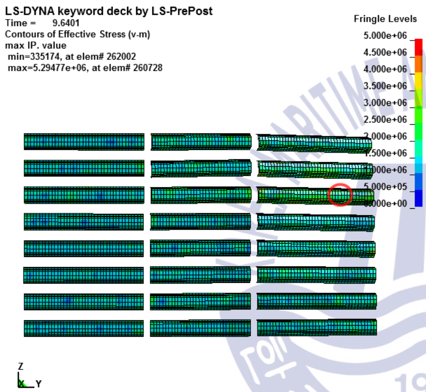

(c) guide rail in 2nd impact

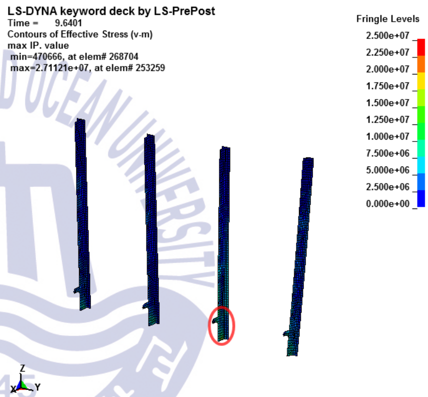

(d) column in 2nd impact

Fig 5.9 von Mises effective stress distributions of guide rails and columns of safety barrier in Case 5

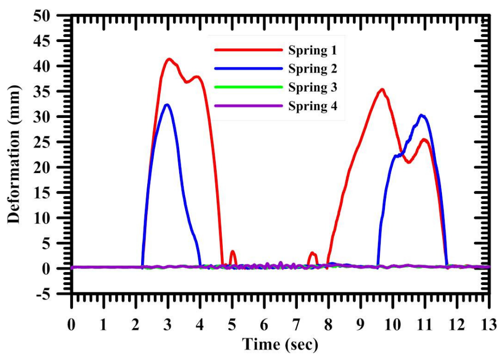

Fig 5.10 Deformation response of spring in hydraulic absorber in Case 5

5.6 Consideration of structural safety assessment of Case 1~5

In the normal impact location, the impact load was transferred to the middle of two columns and the lower guide rails. In the side impact location, the impact load was transferred to the end of column and the lower guide rails, and the maximum von Mises stress and deformation of spring in hydraulic absorber was relatively high. In the upper impact location, to the all the columns and the higher guide rails, the maximum von Mises stress was smaller than normal impact but deformation of spring in hydraulic absorber was almost the same as the normal impact one. In the side and upper impact location, the impact load was transferred to the end of column and the upper guide rails, and the maximum von Mises stress and deformation of spring in hydraulic absorber was the highest in the all scenarios. Therefore, it could be expected more serious damage in the unusual impact loading condition, and more keen attention and careful inspection would be required and more proper handling of weights, such as containers and drill pipes, etc., should be suggested. Through the impact simulation, it could be found that the safety barrier would have the sufficient structural strength in this impact loading cases.

6. Conclusion

These days, the crash accidents frequently occurred unexpectedly between the main equipment and heavy cargos, such as containers and drill pipes, etc., on ship and offshore plant during cargo lifting. To prevent these clash accidents, the safety barrier should be installed around the main equipments, and be back to the its original position by its hydraulic spring-damper system, and be inclined to the small angle under 14° during cargo impact to equipments.

The objective of this study was to develop a more accurate and realistic impact response analysis technique of safety barrier with hydraulic spring-damper absorbers for the structure safety assessment of safety barrier and its improvement to the impact accidents, using LS-DYNA code, by the verification of impact test result in Case 1 and the consideration of diverse impact response analysis in Case 2~5.

The impact simulation of the safety barrier was verified through the comparison of simulation results with test one using diverse damping viscous values of hydraulic absorber and damping coefficients in contact option between the safety barrier and impact medium. Through the impact simulations considering severe impact loading conditions, it could be found that the safety barrier would had the sufficient structural strengths, such as the limitation of the inclined angle 14°, the maximum von Mises effective stress in the safety barrier and the maximum tension deformation in spring component of hydraulic absorber, in the diverse impact loading cases. More serious damage in the unusual impact loading condition would be expected through the structural safety assessment, therefore, more keen attention and careful inspection would be required and more proper handling of weights, such as containers and drill pipes, etc., should be suggested.

References

British Standards, 2007. BS EN 1999-1-1 *Design of aluminum structures*, United Kingdom.

DNVGL, 2010. DNV-OS-C401 *Fabrication and Testing of Offshore Structures*, Norway.

KOMERI, 2016, S2169829-FB-PIT *Impact test procedure for aluminum safety barrier*, Republic of Korea.

LSTC, 2013. LS-DYNA User's Manual, Version R7, *Livermore Soft Technology Corp*, USA.

SEBOTECH, 2016. S2169829-FB-300-001 *Shock Absorber for Flexible Barrier*, Republic of Korea.

Acknowledgement

석사 입학부터 졸업하기까지 항상 올바른 학문의 길로 나아갈 수 있도록 지도하여 주시고 한없이 부족한 저에게 무한한 관심과 지원, 아낌없는 응원을 해주신 이상갑 교수님께 존경을 표합니다. 아직 많이 부족하지만 교수님의 발자취를 열심히 따라 청출어람으로 보답하겠습니다. 교수님 감사합니다.

또한 본 논문을 완성할 수 있도록 지도와 심사를 해주신 박석주 교수님과 남종호 교수님께 감사드리며, 석사과정동안 많은 가르침을 주신 조선해양시스템공학부 교수님들께 감사드립니다.

제가 석사과정을 시작할 때부터 지금까지 항상 따뜻하게 맞아주시고 올바른 조언을 해주신 이재석 박사님, 저와 같이 석사과정을 시작하며 물심양면으로 도움을 준 이환수 씨에게 감사의 말씀을 표합니다. 또한 항상 밝고 친절하게 맞아주는 박지훈 씨와 정태영 씨에게도 감사하다는 말을 전하고 싶습니다. 모두 앞날에 항상 행복만 있기를 기원하겠습니다.

석사과정 동안 많은 도움을 주신 한국조선해양기자재연구원 에너지해양연구본부 김정환 본부장님 시뮬레이션 응용연구센터 최주형 박사님, 유찬욱 팀장님, 배징도 파트장님, 차종국, 김승찬, 이재훈 선임연구원님, 김지선, 김은빈 연구원님에게도 감사드립니다.

마지막으로 진인사대천명의 자세로 정직하고 겸손한 삶을 강조하시는 존경하는 아버지, 타지 생활하는 저에게 격려와 지원을 아끼지 않으시고 아들, 딸을 위해 무조건적으로 희생하시는 어머니, 항상 오빠를 응원하는 동생 은영이, 가족 모두에게 이 논문을 바치며, 항상 감사하고 사랑합니다.